Front. Energy 2020, 14(1): 81–104
https://doi.org/10.1007/s11708-019-0653-8

REVIEW ARTICLE

Junheng FU, Chenglin ZHANG, Tianying LIU, Jing LIU

Room temperature liquid metal: its melting point, dominating mechanism and applications

Abstract The room temperature liquid metal (LM) is recently emerging as a new class of versatile materials with fascinating characteristics mostly originated from its simultaneous metallic and liquid natures. The melting point is a typical parameter to describe the peculiarity of LM, and a pivotal factor to consider concerning its practical applications such as phase change materials (PCMs) and advanced thermal management. Therefore, the theoretical exploration into the melting point of LM is an essential issue, which can be of special value for the design of new LM materials with desired properties. So far, some available strategies such as molecular dynamics (MD) simulation and classical thermodynamic theory have been applied to perform correlative analysis. This paper is primarily dedicated to performing a comprehensive overview regarding typical theoretical strategies on analyzing the melting points. It, then, presents evaluations on several factors like components, pressure, size and supercooling that may be critical for melting processes of liquid metal. After that, it discusses applications associated with the characteristic of low melting points of LM. It is expected that a great many fundamental and practical works are to be conducted in the coming future.

Keywords melting point, liquid metal, crystal, thermodynamics, molecular dynamics

Received Jun. 24, 2019; accepted Sept. 21, 2019; online Dec. 25, 2019

Junheng FU, Chenglin ZHANG
CAS Key Laboratory of Cryogenics, Technical Institute of Physics and Chemistry, Chinese Academy of Sciences Beijing 100190, China; School of Future Technology, University of Chinese Academy of Sciences Beijing 100049, China; Beijing Key Laboratory of Cryo-Biomedical Engineering, Beijing 100190, China

Tianying LIU
CAS Key Laboratory of Cryogenics, Technical Institute of Physics and Chemistry, Chinese Academy of Sciences, Beijing 100190, China; School of Engineering Science, University of Chinese Academy of Sciences Beijing 100049, China; Beijing Key Laboratory of Cryo-Biomedical Engineering, Beijing 100190, China

Jing LIU (✉)
CAS Key Laboratory of Cryogenics, Technical Institute of Physics and Chemistry, Chinese Academy of Sciences, Beijing 100190, China; School of Future Technology, University of Chinese Academy of Sciences, Beijing 100049, China; Beijing Key Laboratory of Cryo-Biomedical Engineering, Beijing 100190, China; Department of Biomedical Engineering, School of Medicine, Tsinghua University, Beijing 100084, China
E-mail: jliu@mail.ipc.ac.cn

1 Introduction

The room temperature liquid metal such as gallium and its alloy is a new kind of important functional material, which owns traditional metallic behaviors like high conductivity, thermal conductivity, and distinctive rheological properties [1]. Compared with the commonly known mercury, gallium based liquid metal has a much low toxicity and a lower vapor pressure [2–4]. Meanwhile, the melting temperature of gallium-based alloys can be modulated by changing the components and sizes. This brings new research value to the modification of metal fusion. Thanks to its special rheological properties and metal properties, low-melting point liquid metal has recently been increasingly used in the thermal control process [5–9], biomedical health care [10–13], microfluidic chips [14–16], fuel cells [17,18], deformation movements [19–22], chemical catalysis [23–25], addictive manufacturing [26,27] and more other fields [28–30] in both macro and micro aspects. The amazing characteristics of such liquid metals make their development both appealing and critical, which is in fact bringing about brand-new perspectives and opportunities for many cutting-edge areas.

With the development of the ultimate coolant formed by the nano-crystallization of liquid metal with a low melting point, it is well-known that the liquid metal nanoparticles became gradually significant in microscale [31]. Some provocative effects in the nano-process of the material like Quantum effect [32], biomimetic phenomenon [33], and

supercooling phenomenon [34], expand the application scope and material dimension of the material. Besides, Ga_2O_3 with a thickness of 0.5–3 nm will be generated on the surface of pure gallium at the presence of trace oxygen, which would change the fusion temperature between pure gallium and oxide [35]. So far, some methods such as particles embedded elastomer electronic skin [36], biological macromolecule material coated liquid metal capsule [37], chemical reagent rapid preparation of long-term, stable liquid metal nanoparticles [38], polymer/liquid metal core-shell structure of energy-saving devices [39], have proven the complementary and superiority of low melting point alloy composites, where solid particles and traditional metal powders fail to applications. On the other hand, the material design, which is to comprehend and research different materials and composite new substances by combining each other's properties, is an emerging area. The resultant substance owns different physical properties from the original material. For instance, the field of high-entropy alloys (HEAs) comprised with kinds of metals, which has some unexpected photo-electronic, ductile, and hyper-elastic properties by the synergistic effect, has been a scientific frontier till now [40,41]. With the breakthrough of research content, it can be expected that liquid metal would lead to a fundamental revolution in both academic and industrial circles in the near future.

For the aforementioned scenarios, liquid metal and its composites play a critical role in practical applications. However, to the best of the authors' knowledge, there are few reports on the fundamental physicochemical parameters of room temperature liquid metal, mainly focusing on material development. The melting point, as the basis for calculation of other physicochemical parameters like the surface tension, vapor pressure, and phase equilibrium, is perhaps the critical factor to identify liquid metals and explore their applications [46]. For example, the difference between macroscopic and microscopic melting point is reflected by the degree of subcooling, and the temperature of phase transition plays a decisive role in the relevant applications [47]. At the same time, it is fatal to choose materials with the applicable melting range in addictive manufacturing industry due to the constraints of instruments and costing.

Under the conditions of Lindemann and Bonn criteria, combining theoretical predictions based on thermodynamic relationships with experimental results is the common approach for obtaining the melting point of materials. In 2013, Wang et al. [48] proposed the liquid metal material genome project so as to guide material synthesis. This requests an overall presentation of theoretical model, influencing factors, and related applications of liquid metal. Zhou et al. [49] measured the composition and melting process of 13 kinds of bismuth-based eutectic alloys by experimental methods, which enriched the experimental data of liquid metals at room temperature. To the best of the authors' knowledge, there is still a lack of overall perceptive of the liquid metal melting process. The existing solution theory cannot explain the melting mechanism of the gallium-based alloy well owning to the special metal bond of the gallium metal.

To systematically understanding the fusion process of liquid metal, a fundamental exploration of the melting

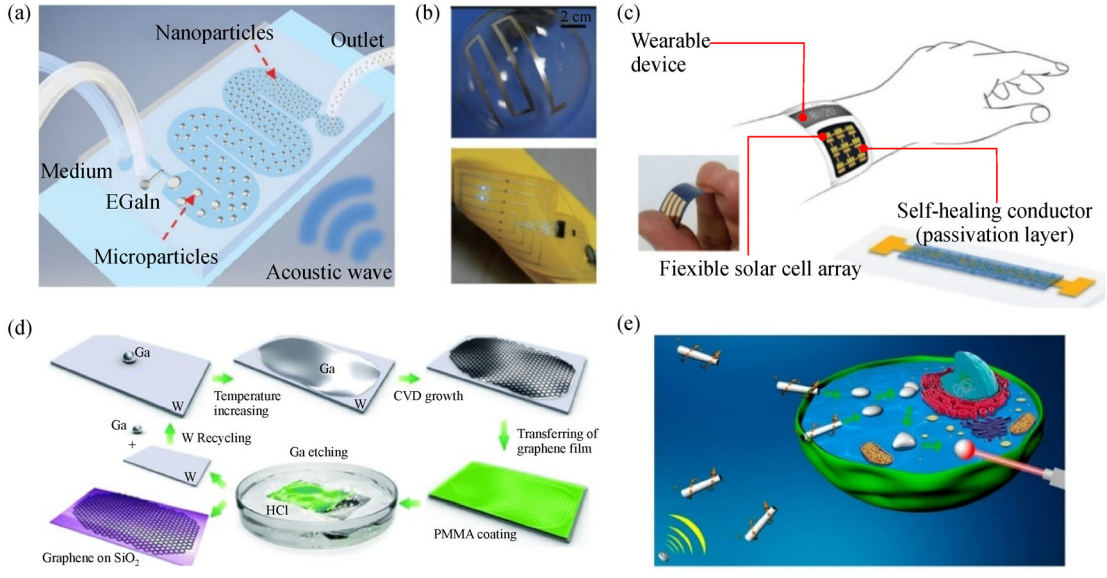

Fig. 1 Typical applications of low melting-point liquid metal.

(a) Microfluidics: fabrication of liquid metal nanoparticle (adapted with permission from Ref. [42]); (b) addictive manufacturing: circuits diagram (adapted with permission from Ref. [26]); (c) wearable devices with self-healing liquid metal conductor powered by solar energy (adapted with permission from Ref. [43]); (d) synthesis of graphene catalyzed by liquid metal (adapted with permission from Refs. [44,45]); (e) tumor therapy enabled by the photothermal property of liquid metal nanoparticles (adapted with permission from Ref. [21]).

point is indispensable. In this paper, the melting point of liquid metal was expounded from three perspectives: the fundamental theory to predict the melting point, typical effects that affect the fusion process, and application areas that may be involved in melting point design. Besides, low melting point alloys and functional materials were discussed. Finally, the current research was summarized and future development was prospected.

2 Fundamental theory

Understanding and mastering the properties of the material would contribute to its further research and application. The melting process, as one of the most important thermal properties of materials, has caused great concern in the field of material and engineering. The theory of calculating the melting point has been well developed. Herein, the criterion for metallic fusion is presented. The fundamental theories are summarized in two directions: the thermodynamic theory from a macroscopic point of view and the molecular dynamic simulation from a microscopic point of view, through which, the theoretical prediction about melting point of metallic substances could be available.

2.1 Criterion for melting process

In 1910, Lindemann proposed the assumption that the atomic motion in the crystal was a simple harmonic motion, which well explained the melting process of crystal [50–53]. According to this theory, the amplitude of the atom near the equilibrium position changes in term of the thermal motion. When the ratio of the root mean square amplitude of the atomic vibration to the atomic spacing R reaches a critical point δ_{L}, the crystal will melt. The δ_{L} at the melting point, which also named Lindemann parameter, is defined as [54]

$$\delta_{\mathrm{L}}^2 = (\langle U^2\rangle / r^2)_{T_{\mathrm{m}}}, \tag{1}$$

where r is the nearest-neighbor distance and $\langle U^2\rangle$ is the mean-square-amplitude of vibration of a monatomic lattice, which in the quasi-harmonic approximation can be expressed in Ref. [55].

The interaction between atoms, which means the process of physical state change, is the change of binding energy between atoms. Therefore, the binding energy between microscopic atoms will be related to the change of the phase of macroscopic materials. According to Lindemann criterion, Fransisco et al. [56] theoretically derived an empirical relationship between binding energy and melting point, i.e.,

$$T_{\mathrm{m}} = 0.032\frac{\Delta E}{k_{\mathrm{B}}}, \tag{2}$$

where ΔE is the cohesive energy at the equilibrium lattice constant, k_{B} is Boltzmann's constant, and T_{m} is the melting point.

Metal melting is not only reflected in the thermal vibration of microcrystalline cells, but also refers to the fact that the macroscopic stiffness will sharply change. From the perspective of the elastic shear modulus of solid, the state that the elastic modulus of solid disappears or mutates is defined as the melting process of the entire crystal [57]. The melting process is often called mechanical melting because crystals do not have enough stiffness to maintain the shape.

Cahn [53] calculated that for most of the particles, rather than the whole crystal, when taking the Lindemann criterion of a critical score of 0.22, Born average elastic shear modulus tends to be zero. Namely, melting is obtained when local lattice is in the state of instability, which is made from the combination of the two standards. This result shows that the two criteria are essentially the same when describing the melting of substance, but from a different perspective. Both melting criteria are usually used in numerical simulations and experiments [58,59].

2.2 Thermodynamic theory

The thermodynamic equilibrium is featured as a state where no macro changes occur over the time. An important conclusion of the classical thermodynamics is that a closed system can be regarded as a state of thermodynamic equilibrium if the system has a minimum value of Gibbs free energy G, where the temperature and pressure are constant (Fig. 2(a)). Such basic conclusions have been applied for the calculation of parameters about phase change processes. Teldes [60] believed that based on the second law of thermodynamics, the latent heat of a substance could be calculated with the melting point of components, and studied several alloys of high melting points that could be used as energy storage materials. Birchenall [61] proposed that equations about the melting points of eutectic alloys could be obtained by using classical thermodynamics under general simplification.

Supposing that microscopic changes have ignorable influences on macroscopic transitions, the melting process of an alloy can be specifically simplified as a two-step process: solid-liquid phase changes of every single component and mixing of different components in liquid phases.

Considering the fact that the proportion of the same component varies in different phases during the transitions of the alloy, the chemical potential about Gibbs free energy is needed, which is defined as

$$\mu_{\mathrm{B}} = \left(\frac{\partial G}{\partial n_B}\right)_{T,p,n_{\mathrm{C}}}. \tag{3}$$

For further calculation, the equation for the chemical potential of a certain substance in liquid phase can be

written as

$$\mu_{\mathrm{M}}^{\mathrm{L}} = G_{\mathrm{M}}^{\mathrm{L}} + RT\ln a_{\mathrm{M}}^{\mathrm{L}} = G_{\mathrm{M}}^{\mathrm{L}} + RT\ln x_{\mathrm{M}}^{\mathrm{L}} + RT\ln\gamma_{\mathrm{M}}^{\mathrm{L}}, \quad (4)$$

where μ is the chemical potential, G is the Gibbs free energy, x is mole fraction of the substance M, a is activity, and γ is activity coefficient. The superscript L represents the liquid phase. The calculation for the chemical potential of the substance in solid phase is the same as Eq. (4).

When dealing with phase change processes, the difference of Gibbs free energy G between each phase at temperatures away from that of the equilibrium state (Fig. 2(b)) is often focused on. The deviation of G from that of the stable state leads to the change of G, providing driving forces for the transition (Fig. 2(c)). Based on classical thermodynamics, when a substance reaches equilibrium in different phases, chemical potentials from all phases are the same. Subsequently, the end about transition of the alloy is the certain moment when chemical potentials of the alloy in solid and liquid phases are equal. For calculation, the criterion is that chemicals of every component in solid and liquid phases from the alloy are the same.

According to the above analysis, parameters about the phase change can be obtained through calculation. To be exact, the values of Gibbs free energy change ΔG_{mix} are of first importance in calculation (Fig. 2(d)). A common hypothesis ideal liquid mixture is introduced here to simplify the calculation. The formulas thus established can be used for realistic situations after modification. If the alloy is considered to be an ideal liquid mixture, the following desirable properties can be obtained [62]:

(1) The volume of the mixture is equal to the sum of the

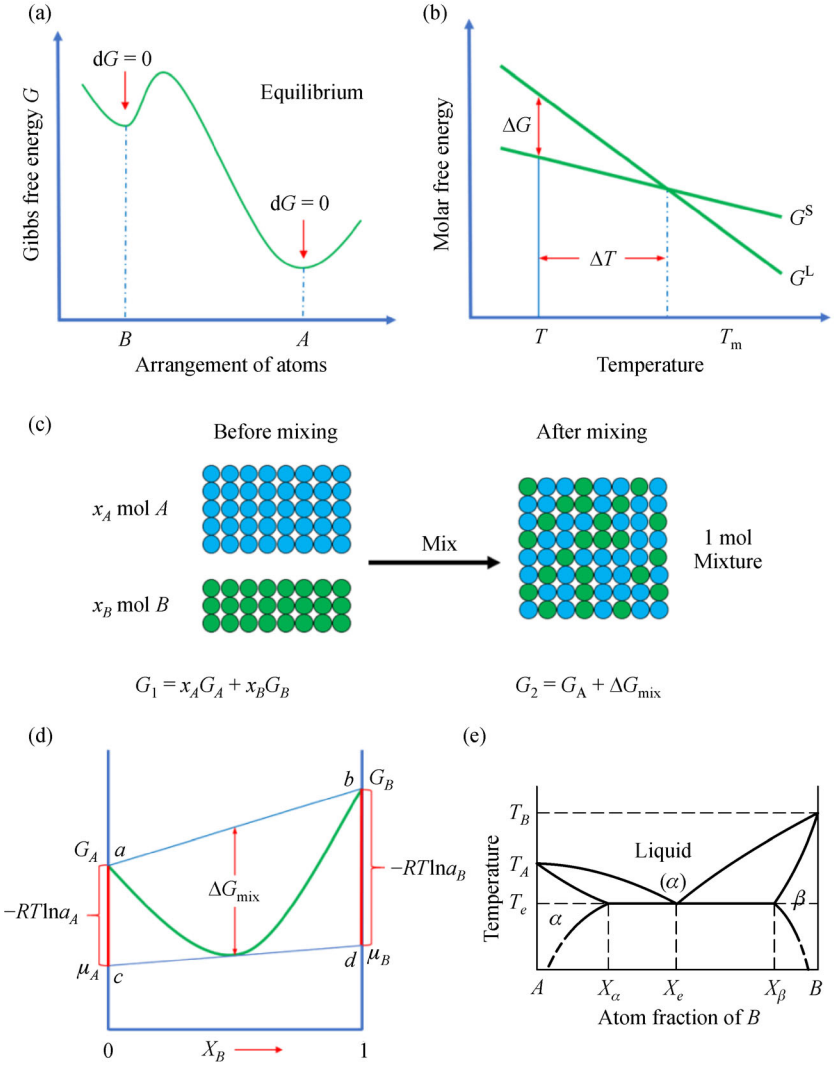

Fig. 2 Typical schematics about Gibbs free energy, chemical potential and phase diagrams (adapted with permission from Ref. [60]). (a) Changes of Gibbs free energy with the different arrangements of atoms (Systems with structure 'A' is at stable equilibrium while those with structure 'B' is at metastable equilibrium.); (b) molar free energy for the substance of different phases;(c) Gibbs free energy change during mixing for a binary system;(d) relationship between Gibbs free energy and chemical potential for binary solutions; (e) phase diagram of eutectic binary systems.

volumes of the pure components before mixing;

(2) The enthalpy of mixing between two pure liquids is zero; and

(3) The system has an ideal entropy of mixing.

In addition, the chemical potential of a single component in the mixture is much easier to calculate. Through such an assumption, Pan et al. [63] obtained equations for the melting point and latent heat of binary, ternary and quaternary alloys (Eq. (5)), the values got from which showed slight differences compared with those experimental values. They also proposed the calculation strategy for alloys with more components. Therefore, the melting point of an alloy is feasible to predict based on thermodynamics, i.e.,

$$\ln\frac{a_{\mathrm{M}}^{\mathrm{L}}}{a_{\mathrm{M}}^{\mathrm{S}}} = -\frac{L_A}{R}\left(\frac{1}{T_{\mathrm{m}}}-\frac{1}{T_A}\right). \tag{5}$$

Considering the relationships among Gibbs free energy, temperature, pressure, and composition, phase diagrams can be drawn based on a large amount of thermodynamic data. Through the phase diagram, the information of the Gibbs free energy change can be intuitively obtained, thus judging the point of phase transition and obtaining related parameters. Van Larr [64] first proposed the CALPHAD (calculation of phase diagrams) in 1908. Since the 1970s, with the development of thermodynamics, statistical mechanics, solution theory, and computer technology, phase diagram research has entered a new stage of coupling between computer and thermochemistry [65]. Using the CALPHAD method, based on thermodynamic knowledge and existing data, difficulties in conducting some actual experiments can be possibly avoided. Besides, it is possible to predict the phase diagram of the system, or estimate the experimentally difficult parts by the easy-to-measure part to improve the accuracy [66–68] (Fig. 2(e)). However, the CALPHAD method is supported by a large thermodynamic database, and experimental measurements of the necessary parameters are indispensable.

The thermodynamic-based approach undoubtedly provides a simple and feasible tool for estimating the melting point of an alloy. However, differences between this idealized operation and the real system must be emphasized. Usually, mixing is an endothermic or exothermic process, and the enthalpy of mixing is impossible to be zero for ordinary solution systems. Therefore, it is essential to consider the enthalpy of mixing [69]. According to the quasi-chemical model, the enthalpy of mixing ΔH_{mix} only depends on the bond energies of adjacent atoms. The above method can be modified with this model. However, the model is established on the assumption that the volumes of different pure components are the same, which also do not change during mixing, so that the interatomic distances and bond energies are independent of the composition [70].

This modification, however, is still unable to accurately describe the dependence of Gibbs free energy change ΔG_{mix} on temperature and composition during mixing for real systems. A steady-state is not solely guaranteed by the random arrangement of atoms, while the actual arrangement of atoms must match the change to achieve an available minimum ΔG_{mix}. Meanwhile, the entropy increases as temperature increases, which, in turn, reduces the order of the atoms inside the material. Assumptions about atomic arrangements and bond energies from the quasi-chemical model neglect all these complex details. Additionally, for some systems with strong chemical bonds inside, the mixture of phase changes will even break the lattice structure of the original pure components, and obtain the intermetallic phase with a highly ordered structure [70]. For these complex authentic changes, the accurate calculation about the enthalpy of mixing ΔH_{mix} needs to be further considered.

2.3 Molecular dynamics simulation

Molecular dynamics simulation is a numerical calculation method that simulates a multi-body system composed of nuclei and electrons, and thus obtains the structure and properties of the system. With the development of computing performance, molecular dynamics simulation has become an important method for material design and property prediction.

In a molecular dynamics simulation, the system is described by Newton's equation of motion. By solving the differential equation of Newton's Second Law, the details of the motion of the atom can be obtained by Eq. (6) [70], i.e.,

$$a_i = \frac{\mathrm{d}^2\boldsymbol{r}_i}{\mathrm{d}t^2} = \frac{\boldsymbol{F}_i + \boldsymbol{f}_i}{m_i}, \tag{6}$$

where m_i, $\boldsymbol{r}_i$, $\boldsymbol{F}_i$, and $\boldsymbol{f}_i$ are the mass of the ith atom, the position vector, the force from the potential field, and other forces, respectively, in which $\boldsymbol{F}_i$ can be calculated according to the gradient of the potential function $\boldsymbol{F}_i = -\nabla_i U$.

The accuracy of the interaction potential between atoms has a great influence on the accuracy of the calculation results. The potential function model proposed can be roughly divided into the pair potential and many-body potential. The pair potential model believes that the interactions among atoms are in pairs, independent of the positions of other atoms, while many-body potential considers the interaction effects of other atoms. Embedded-atom method (EAM) is one of the most widely used models, which is a semi-theoretical many-body potential model. The basic idea of the EAM potential is to divide the total potential energy of the crystal into two parts. One part is the interaction between the nucleus on the lattice. The other part is the embedding energy of the nucleus embedded in the background of the electron

cloud, which represents multi-body interaction. In this way, the total potential energy of the system can be expressed as [71]

$$U = \sum_i F_i(\rho_{h,i}) + \frac{1}{2}\sum_{i\neq j}\phi_{ij}(R_{ij}), \tag{7}$$

where F_i is the embedding energy, $\rho_{h,i}$ is the total density of the electron of other atoms except the atom at $R_{i,j}$ position, which can be expressed as $\sum_{j\neq i} f_j(R_{ij})$.

The potential function ϕ_{ij} here uses the Johnson potential, which is an interatomic potential model and has superiority in describing metal crystals.

$$\phi_{i,j}(R_{i,j}) = -A_n(R_{i,j}-B_n)^3 + C_nR_{i,j}-D_n. \tag{8}$$

It should be pointed out that the form of the embedding energy $F_i(\rho_{h,i})$ and the interatomic potential function $\phi_{ij}(R_{ij})$ are not unique. The function listed is just the classic model. There is still a lot of ongoing research work to modify the EAM model [72,73].

The energy and temperature relationship of the system can be calculated when the potential energy function is determined. Normally, the melting point of a nanocluster can be obtained by calculating its potation energy as a function of temperature. The melting point appears when energy jumps sharply (Fig. 3(a)). Another way to determine the melting point is to calculate the relationship between the Lindemann index and temperature. The local Lindemann index of the ith atoms (δ_i) for a system of N atoms is defined as the root-mean-squared bond length fluctuation, i.e.,

$$\delta_i = \frac{1}{N-1}\sum_{j\neq i}\frac{\sqrt{\langle R_{ij}^2\rangle - \langle R_{ij}\rangle^2}}{\langle R_{ij}\rangle}. \tag{9}$$

The system of averaged Lindemann index is expressed as

$$\delta = \frac{1}{N}\sum_i \delta_i. \tag{10}$$

According to the Lindemann criterion, fusion occurs when the index is ranging from 0.1 to 0.15, and it is related to the type of material. Yang et al. [59] studied the nanoparticles of Pb and Li, and compared the difference between the potential energy and the Lindemann index.

Molecular dynamics are now widely used in theoretical studies of physics, chemistry, and biological systems. It provides a very effective method for material design and performance prediction. It should be pointed out that

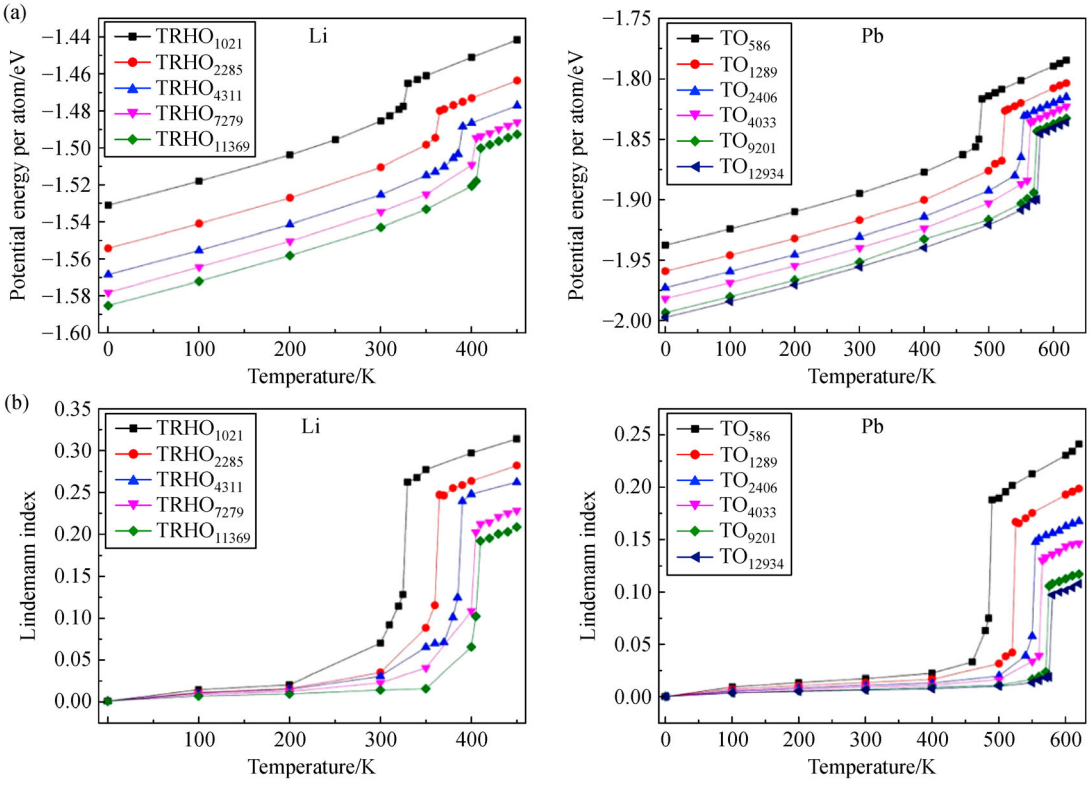

Fig. 3 Molecular dynamic simulation results judged by various criteria.
(a) Variations of the potential energy per atom; (b) Lindemann index (adapted with permission from Ref. [59]).

the current molecular dynamics simulation is mainly to calculate nanoclusters, and there is nothing to do with the bulk. The relationship between the melting point of bulk and nanocluster will be explained in detail in Section 3.

3 Calculation method of the melting-point of liquid metals

Due to the huge difference in hardness from conventional metals, research on the basic physical properties of liquid metals, including melting points, has been conducted for a long time, from theoretical calculations to experimental investigations and mathematical statistics. Herein, the various techniques that interpreted the melting process of the several common liquid metal elements and their alloys will be presented.

3.1 Mercury

As the only liquid metal in natural environment with large density, mercury is the first liquid metal known and utilized by humans with a melting point of 234 K [74,75]. Its abnormal physical properties have attracted much attention. Norrby [76] summarized the scientific explanations of liquid origin of mercury from the perspective of relativistic effect and anomalies compared with the chemical properties of gold, the adjacent elemental. Due to the relativistic effect and lanthanoid contract, the two 6s electrons in Hg contribute less to the metal-metal bonds than that of metal gold, making the melting point of mercury much lower than the next-door neighbors. Calvo et al. [77] began with a microscopic explanation of the anomalous nature of the low melting point of mercury. Using the Monte Carlo (MC) simulation with the quantum diatomics-in-molecules (DIM) model, the interactions among mercury atoms,

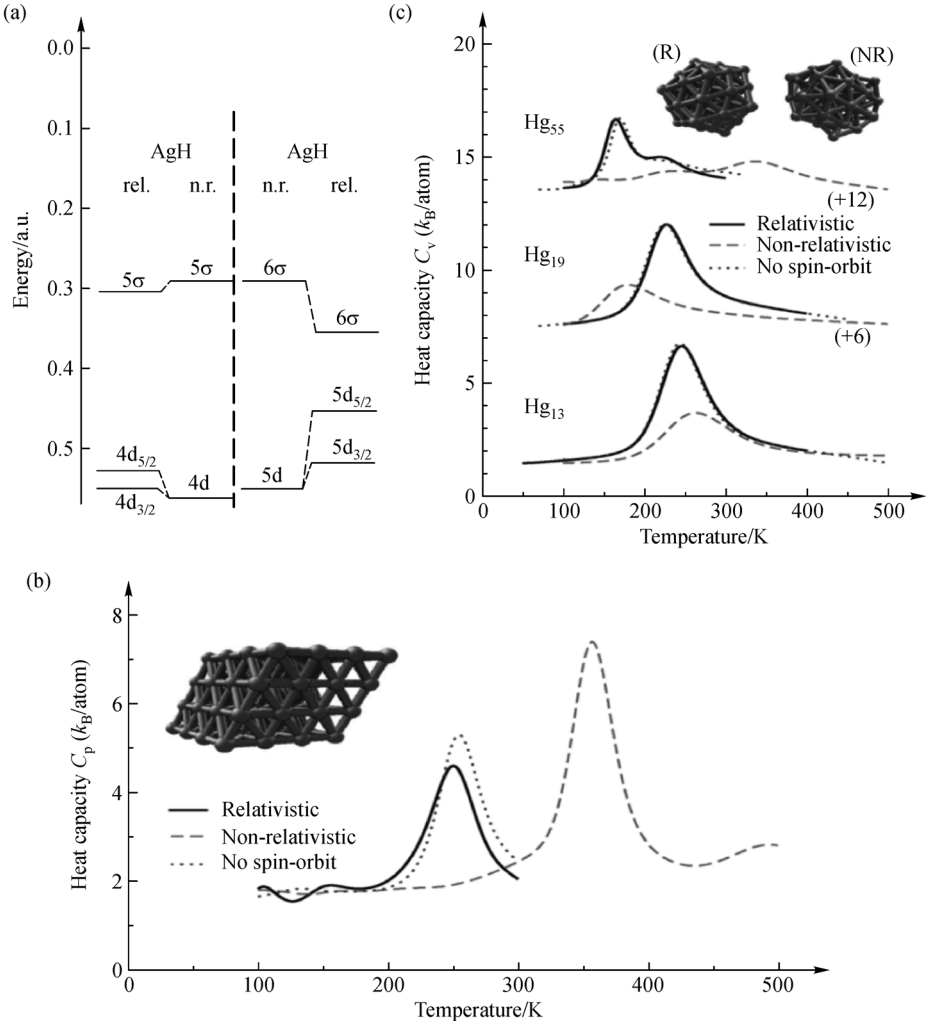

Fig. 4 Illustrations of melting process for mercury.
(a) Differences in electron distribution between gold (Au) and mercury (Hg) (adapted with permission from Ref. [76]); (b) and (c) relativistic effects on the melting process of mercury clusters (adapted with permission from Ref. [77]).

clusters, and bulk mercury and heat capacity under the influence of relative effects were analyzed for the first time. The potential energy curve of the mercury dimer is less affected by the relative effect, and the bond energy shrinkage is only 0.20 Å. However, for the melting process of the many-body interaction states, it would become more and more complicated. As shown in Fig. 4(c), the atomic clusters of different primary and secondary magic numbers such as 13, 19, and 55 are under the influence of relative effects. The melting process has been changed and the maximum temperature difference can reach 176 K (Hg 55). At a constant zero pressure and under a suitable periodic boundary condition, the melting point of the bulk mercury is drastically reduced, and an accurate melting point is obtained at a temperature of 234.32 K in consideration of the relative effect. Conversely, regardless of the relative effect, there is a mistake in the presence of solid mercury at room temperature.

3.2 Gallium

The room temperature liquid metal gallium and its alloys are attracting significant attentions as rheological, non-toxic, non-volatile which are used to be alternative applications of mercury. In the following, the melting process of the gallium-based liquid metals with respect to the theoretical derivation, numerical simulation, experimental research and environmental conditions, which is consistent with the basic theoretical framework of the second part, is discussed.

The melting process of gallium single crystals has a significant correlation with the lattice structure. Quantitative research on the melting process of metal gallium, the traditional theory of melting caused by impurities, indicates that there is a deviation with the results of the gallium. The dislocation phenomenon inside the metal induces the melting of gallium, and the vibration of the line defect in the vicinity determines the acoustic and thermodynamic properties [78,79]. At a slow heating rate, rather than a rapid temperature rise, the melting of metal gallium does not feature a stable fixed melting point, but rather multiple melting processes on different crystal phases [80,81].

The numerical simulation method has also been used to study the solid-liquid phase transition of gallium for many years. Bridgman [82] first measured solid gallium with X-ray diffraction (XRD), indicating that there were 8 atoms in the gallium cell at atmospheric pressure, and α-Ga was a stable phase. Using the Ab initio molecular dynamics model, the calculation confirmed that there was a significant covalent existence in α-Ga, which led to the density of states at the Fermi energy in α-Ga reduced [83,84]. Bernasconi et al. [85] used Ab initio calculations to analyze the solid structure of gallium. The presence of α-Ga interpreted the anisotropy of its thermal properties (conductivity, thermal conductivity). In addition, due to the loose, oriented bonding structure, the volume of the gallium shrinks by 2.9% in the melting process [86].

Moreover, experimental measurements are the common method to obtain the melting process of metal. Differential scanning calorimeter (DSC) is a frequently-used device due to its wide temperature range and versatile applications in thermophysical parameters [87,88]. He et al. [89] found that the phase structures of gallium had a relation with the volumes of gallium particles. From the results of DSC, gallium particles with different sizes are corresponding to the different phases. Kumar et al. [90] measured the melting process of the gallium particles in the micro and sub-micron sizes. The resultant illustrated that the melting point of the mciro/sub-micron particles were lower than that of bulk gallium and decreased with decreasing the sizes of the particles.

The melting points of gallium will vary with melting environments. Chen et al. [91] proposed to adjust the lattice boundaries of materials by external field stimulation to obtain suitable soft materials. With gallium melted in porous glass, it is found that there is melting latent heat peak at 230 K, far below the melting point of 302.9 K, where there would be freezing-melting hysteresis related to the order of atoms [34]. In the external rotating magnetic field, the thermal and physical transfer process of gallium in a square container was numerically and experimentally studied [92,93]. Yang et al. [94,95] conducted a dimensionless analysis and simulation of the high *Ra* number of low-melting phase change metal materials, and proposed a new and improved method to measure the thermal properties of the materials.

3.3 Gallium-based alloys

Ga-based alloys are available in a wide variety of liquid temperature zones, making them suitable candidates for a wide range of applications by adjusting the alloy composition to achieve the desired melting point to meet the requirements. For the common eutectic gallium-indium alloy (EGaIn), the X-ray diffractometer measured the liquid structure at room temperature and obtained the structural factor. As shown in Fig. 5, by calculating the double-body distribution function curve of the eutectic gallium-indium alloy and verifing by comparison with pure gallium, the atomic cluster structure of the alloy is modeled, where the In atom is at the center and eight Ga atoms are at the apex to form a simple cubic structure. They are interconnected in a co-angular manner to form larger clusters, and the arrangement and orientation between the clusters do not have a long-range order [96]. Besides, the sharply peak presented the failure of the mechanics of the alloy. According to the Borning's criterion, that peak is the melting point.

Based on the thermodynamic relationship, Eq. (5) illustrated that the melting process of alloys is concerned with the latent of the substance. This formula, however, is

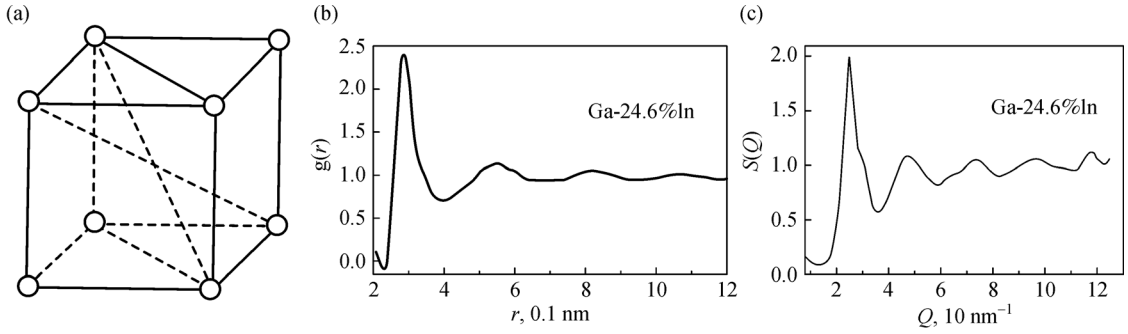

Fig. 5 Structural factors, binomial distribution functions, and cluster models for Ga-In alloys (adapted with permission from Ref. [96]).

accurate to binary alloys. Therefore, for the melting point of ternary and above gallium-based alloys, the experimental methods are frequently used to calculate the melting process due to the complexity of the thermodynamic relationship and the accuracy of the numerical solution. Xiao et al. [97] studied the phase transition behavior of Ga-In-Sn ternary alloy and Ga-In-Sn-Zn quaternary alloy, and found that gallium-based multi-alloys generally underwent metastable state during cooling. Besides, Yu et al. [98] developed a new quaternary GaInSnZn (GISZ) liquid metal with a melting point of 9.7°C, which can reduce the melting and expand the applications of the gallium-based alloys at the present of the zinc element. The DSC curves of different gallium-based alloys are displayed in Fig. 6.

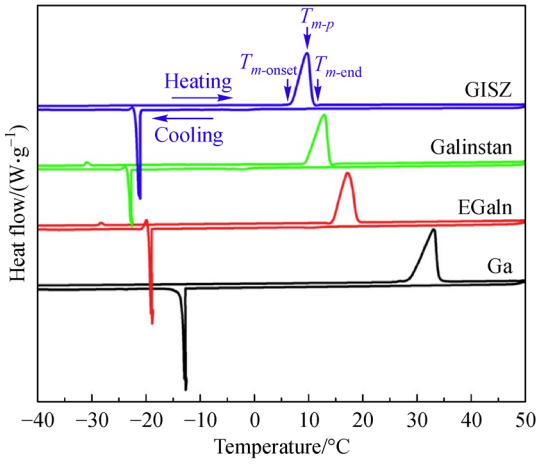

Fig. 6 DSC curves of Ga, EGaIn, Galinstan, and GaInSnZn alloys (adapted with permission from Ref. [98]).

4 Influencing factors for melting point of liquid metals

The reduction of free energy is the essential cause of the solidification process of liquid phase gallium, and the important characterization of nucleation is supercooling. Strictly speaking, the pure metal subcooling can reach 0.56 T_m [99]. Up to now, the measured lowest supercooling of pure gallium, however, is 150 K in epoxy resin due to the heterogeneous nucleation occurs [100]. In addition, compared with other traditional pure metals, gallium, indium and tin contain covalent bonds inside, which makes the system more stable. In the melting process, covalent bonds need to absorb more energy so that they can produce larger supercooling.

4.1 Components

The component of the alloy is an important factor affecting the melting point. In general, the melting point of the alloys is lower than their corresponding pure metals. The reason for this is that the different sizes of atoms in an alloy allow their arrangement less regular than the pure metal, which makes the bonds between the atoms weaker, and reduces the temperature of fusion. Liquid metal with different contents has been systematically studied by theoretical analysis and experimental testing. Common components such as In, Sn, and Zn, are used to form alloys with gallium, which can be miscible with gallium in different ratios to form alloys with various fusion temperature. Phase diagrams of these binary metals are shown in Fig. 7, from which the components of the eutectic alloys can be obtained [101].

Changing the ratio of these alloys can obtain their hypoeutectic and hypereutectic properties, respectively. Referring to the phase diagram, the state of the alloy and the phase composition at different temperatures can be predicted using the lever rule, which has value in material designing.

In addition to these binary alloys, there are some commonly used multi-component liquid metal alloys. The phase transition of multi-alloys is more complicated than that of binary alloys. The melting point and phase transition information of common multi-component alloys including heavy metal elements (Cd and Pb) are just summarized (Table 1).

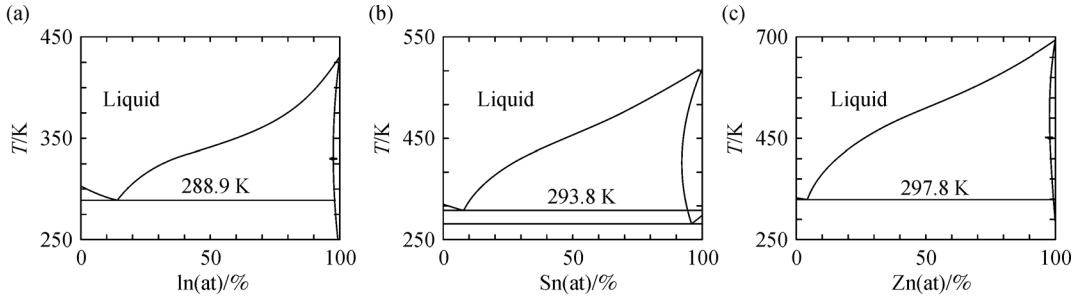

Fig. 7 Phase diagrams.
(a) Ga-In alloy where the atomic mass fraction of indium is 14.2%; (b) Ga-Sn alloy where the atomic mass fraction of tin is 7.7%; (c) Ga-Zn alloy where the atomic mass fraction of metal zinc is 3.9%.

Table 1 Composition, latent heat, and melting point of multi-component liquid alloys [49]

Alloy/(w.t%)	Melting point T_m/°C	Latent heat L/(kJ·kg^{-1})	Type
$In_{25.2}Sn_{17.3}Bi_{57.5}$	80.70	32.47	Eutectic
$In_{51.34}Sn_{5.56}Bi_{33.1}$	60.42	24.34	Eutectic
$In_4Sn_{40}Bi_{56}$	101.13	3.87	Near-eutectic
$Sn_{22}Bi_{50}Pb_{28}$	97.06	17.55	Near-eutectic
$Sn_{22}Bi_{52.5}Pb_{32}$	96.84	21.64	Near-eutectic
$Sn_{26}Bi_{53}Cd_{21}$	92.55	2.52	Near-eutectic
$Bi_{51.6}Cd_{8.2}Pb_{40.2}$	92.97	26.66	Eutectic
$Sn_{51.2}Cd_{30.6}Pb_{18.2}$	144.99	40.6	Near-eutectic
$In_{10.5}Sn_{19}Bi_{53.5}Pb_{17}$	60.66–76.18	16.91	Not eutectic
$In_{21}Sn_{12}Bi_{49}Pb_{18}$	59.73	27.07	Eutectic
$Sn_{13.3}Bi_{50}Cd_{10}Pb_{26.7}$	72.14	30.35	Eutectic

4.2 Pressure

Generally, the melting point of a material increases as the pressure increases. The method to change the melting temperature by pressurization has a practical value for some phase change material (PCM). The devices thus designed include some contact junctions that can create a high pressure, as shown in Fig. 8. In the heating process, these high pressure areas can retain a part of the solid crystals, which can be used as nucleation to reduce the supercooling in solidification [102,103].

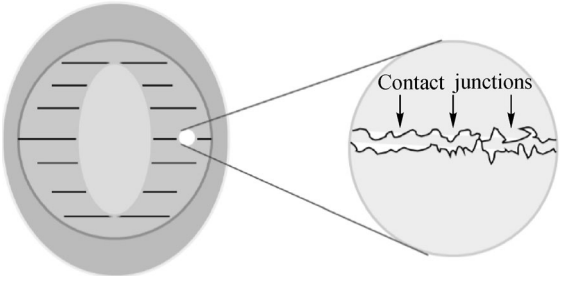

Fig. 8 Structure of a commercial reusable heat pack (Solid crystals can easily be trapped at the contact junction with high pressure.)

The relationship between melting point and pressure can be described by Clausius-Clapeyron's equation [104], i.e.,

$$\frac{\mathrm{d}P}{\mathrm{d}T}=\frac{\Delta H_{\mathrm{f}}}{T\Delta V}=\frac{\Delta S}{\Delta V}. \tag{11}$$

For liquid metal such as gallium, the relationship between pressure and melting point is complicated because gallium exhibits different crystal structures at various pressures. Jayaraman et al. [105] had conducted experiments on the relationship between pressure and melting point of gallium, and obtained the data as shown in Fig. 9.

It can be seen from Fig. 10 that the melting point of gallium does not increase linearly with increasing pressure, which emerges at the two inflection points in the curve. The first inflection point occurs at a pressure of 11.7 kbar (Abnormally, in the interval less than this pressure, the melting point decreases with increasing pressure), the second inflection point appears at 30.0 kbar. The complete curve of gallium is shown in the three-phase diagram of gallium. Figure 10(a) illustrated the three-phase diagram of gallium, which is determined by the DTA and volume change [105]. The results indicate two triple points of gallium. The triple point of liquid – Ga I – Ga II located at

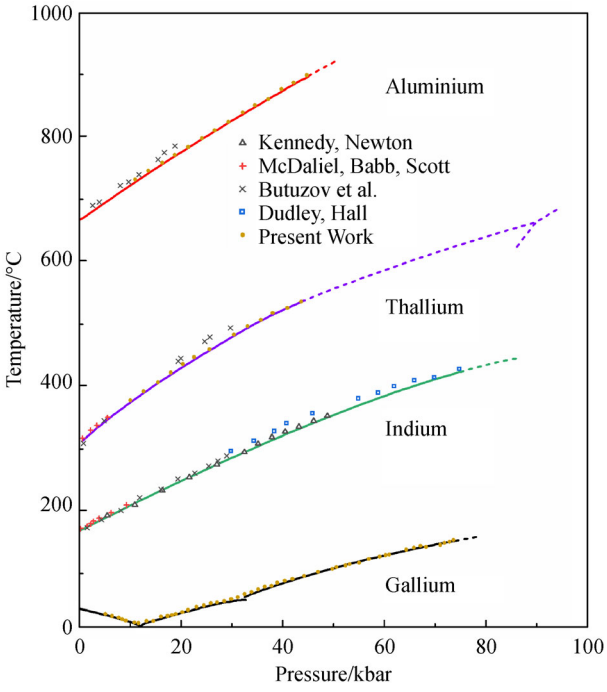

Fig. 9 Melting curves of gallium, indium, thallium, and aluminum (It can be seen that the melting point increases with the increase of pressure except for gallium.) (adapted with permission from Ref. [105]).

11.7 kbar and 3°C, the triple point of liquid- Ga II- Ga III located at 30.0 kbar and 45°C. Ga I is a steady-state phase at atmospheric pressure and is now often called α-Ga. The crystallographic data of α-Ga, Ga II, and Ga III are shown in Table 2.

When the pressure is less than 11.7 kbar, the solidification process of liquid gallium tends to form α-Ga, and the melting point of α-Ga will decrease abnormally with the increase of pressure, whose calculated slope dT/dP is −3.22°C/kbar. When the pressure is between 11.7 kbar and 30.0 kbar, the solidification process of liquid gallium tends to form Ga II. As the pressure exceeds 30.0 kbar, the solidification process of liquid gallium tends to form Ga III. The melting points of Ga II and Ga III increase as the pressure increases in these two regions. The calculated slope dT/dP are 2.29°C/kbar and 2.75°C/kbar, respectively.

The phase diagram in Fig. 10(a) only shows the steady-state phase of the corresponding region, and the possibility of generating transient phases of other crystal forms is not excluded. Defrain et al. [105] observed that the transient phase Ga II may be generated at −16.3°C in the atmospheric environment. In addition, there may be metastable phases such as β, γ, δ, and ε at atmospheric pressure [85]. Table 3 tabulates the parameters of α-Ga and some metastable phases. The possible metastable equilibrium phase boundaries are exhibited in Fig. 10(b).

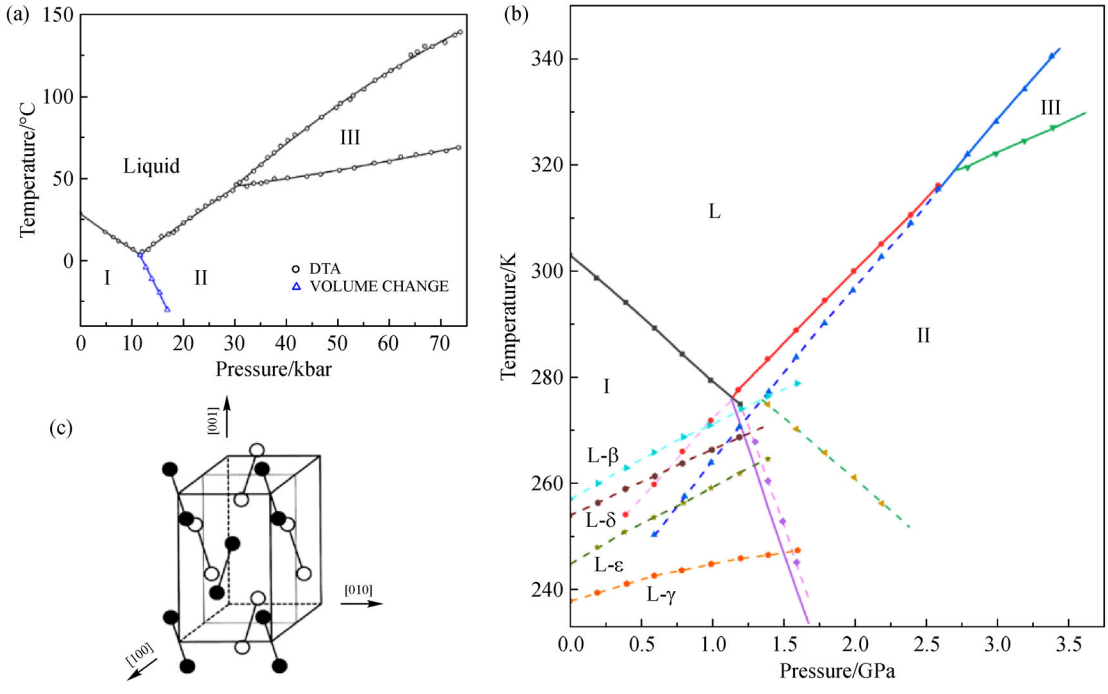

Fig. 10 Phase transition state and structure of gallium.
(a) Three-phase diagram of gallium, which includes two triple points (adapted with permission from Ref. [105]); (b) equilibrium phase diagram of gallium with metastable phase contained (adapted with permission from Ref. [106]); (c) crystal model of α-Ga (adapted with permission from Ref. [107]).

Table 2 Comparison of α-Ga, Ga II, and Ga III [101]

Phase	Crystal system	*a*/Å	*b*/Å	*c*/Å	Ref.
α-Ga	Orthogonal	4.523	4.524	7.661	[108]
Ga II (2.6 GPa, 313 K)	Cubic	5.951±0.005	–	–	[106]
Ga III (2.8 GPa, 298 K)	Tetragonal	2.813±0.003	–	4.452±0.005	[106]

Table 3 Comparison of α-Ga, β-Ga, γ-Ga, and δ-Ga (at atmospheric pressure) [101]

Phase	Melting point /°C	ΔH/(kJ·kg^{-1})	Crystal system	Lattice parameters			
				a/Å	*b*/Å	*c*/Å	Angle
α-Ga	29.78	80.0	Orthorhombic	4.523	4.524	7.661	–
β-Ga	–16.30	38.0	Monoclinic	2.766	3.332	8.053	β = 92.03°
γ-Ga	–35.60	34.9	Orthorhombic	5.203	10.593	13.523	–
δ-Ga	–19.40	37.0	Rhombohedral	7.729	–	–	α = 72.02°

In addition, the anomalous relationship between pressure and melting point of α-Ga would be related to its complex crystal structure. In the α-Ga crystal, the gallium atoms are bonded in pairs, and the interaction with other atoms is weak, thus forming a Ga_2 molecular structure, as shown in Fig. 10(c) [105]. This complex structure may interpret some abnormal physical phenomena, such as low melting point, supercooling, the increased density and the decreased resistivity during melting.

4.3 Size effort

The melting process of bulk substances is weakly related with the size. Only at the nanoscale can the size effect of the melting point be apparently observed. Compared with bulk gallium, it was found that the melting point of gallium micron particles with a diameter of 0.45 μm was approximately reduced by 1 K (T_m = 27.9°C), while the gallium nanoparticles with a diameter of 35 nm were reduced to −14.2°C [9] (see Fig. 11).

Qi et al. [110] proposed Eq. (12) to explain the variation of the melting point of nanoparticles.

$$T_{mp} = T_{mb}\left(1-\frac{N}{2n}\right), \tag{12}$$

where T_{mp} is the melting point of the nanoparticle, T_{mb} is the melting point of the corresponding bulk material, N is the number of atoms on the surface of the nanoparticle, and n is the total atomic number of the nanoparticle.

In Eq. (12), the atoms of the particle are divided into two parts, internal atoms and surface atoms. The cohesive energy per atom of the surface atoms is only half of the internal atoms, since half of the total bonds of each surface atom are dangling bonds. Moreover, the cohesive energy determines the melting temperature. The ultra-high specific surface of the nanoparticles causes the cohesive energy to decline, thus decreasing the melting point. Equation (12), however, ignores the internal relaxation of the nanosolids and does not take into account the shape effects of the nanoparticles. The value of the N/n plays a crucial role. When the shapes of nanosolids are simplified into spherical and disc-shaped assumptions, the value N/n has the

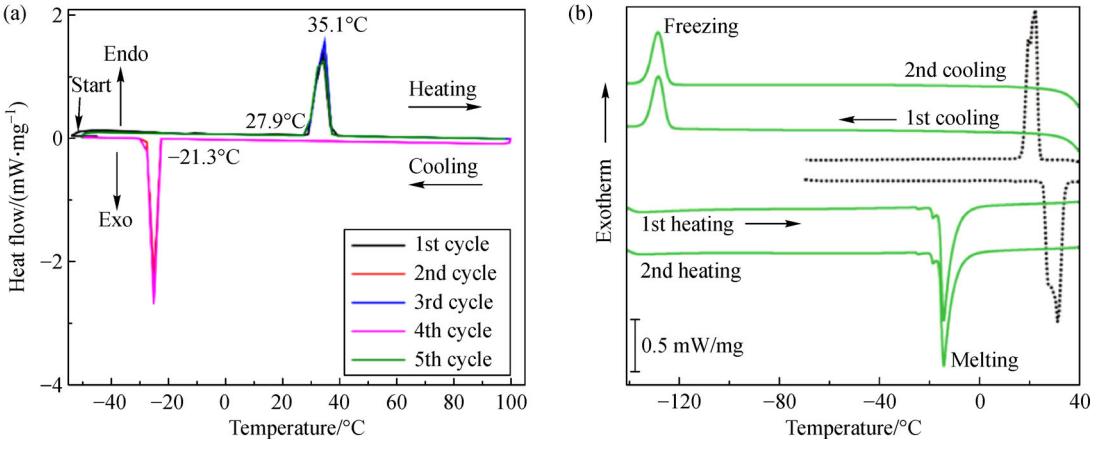

Fig. 11 Characteristic DSC curves of bulk gallium and gallium particles.
(a) Microparticles (> 0.45 μm); (b) nanoparticles (35 nm) (adapted with permission from Ref. [109]).

Table 4 Calculated N/n for different nanosolids [110]

Nanosolid	N/n
Spherical nanosolids	$4d/D$
Disk-like nanosolids	$(4/3)d(1/H + 2/D)$
Nanowires	$(8/3)d/D$
Nanofilms	$(4/3)d/H$

Notes: d—Atomic diameter; D—diameter of the spherical, discotic nanoparticles; H—height of the discotic nanoparticles

following relationship as presented in Table 4. Based on the calculated method, the theoretical calculation of melting process of Sn, Pb, and In primely agree with the testing results (Fig. 12).

In addition, Nanda et al. [111] deduced similar results. The spherical melting point of nanoparticles, nanowires, and nanofilms are $T_m = T_{mb}(1–\beta/D)$, $T_m = T_{mb}(1–2\beta/3D)$, $T_m = T_{mb}(1–\beta/3H)$. Here β is a constant with respect to the material, and $\beta = 3.36$ nm for gallium.

Different from the perspective of cohesive energy, Luo et al. [112] proposed another model based on the change of free energy of the system, which described the principle that the free energy of the system tends to stay at low position. The free energy of the solid and liquid phases is variational at different temperature, and the melting temperature of the nanoparticle can be obtained from the intersection of these free energy curves, as displayed in Fig. 13(a).

Luo et al. [112] divided total Gibbs free energy G_{total} of materials with nanostructure in unit mole as a sum of the volume free energy G_{bulk} and the surface free energy $G_{surface}$ (Eq. (13)). And the area changes of surface A and surface tension γ were considered when calculating surface energy $G_{surface}$ (Eq. (14) and Table 5), i.e.,

$$G_{total}(T) = G_{\partial}(T) + G_{surface}(T) = G_{bulk}(T) + \gamma(T)A(T), \tag{13}$$

$$\gamma(T) = \gamma_m - \frac{d\gamma}{dT}(T - T_{mb}). \tag{14}$$

The molar volumes of the solid and liquid phases as a

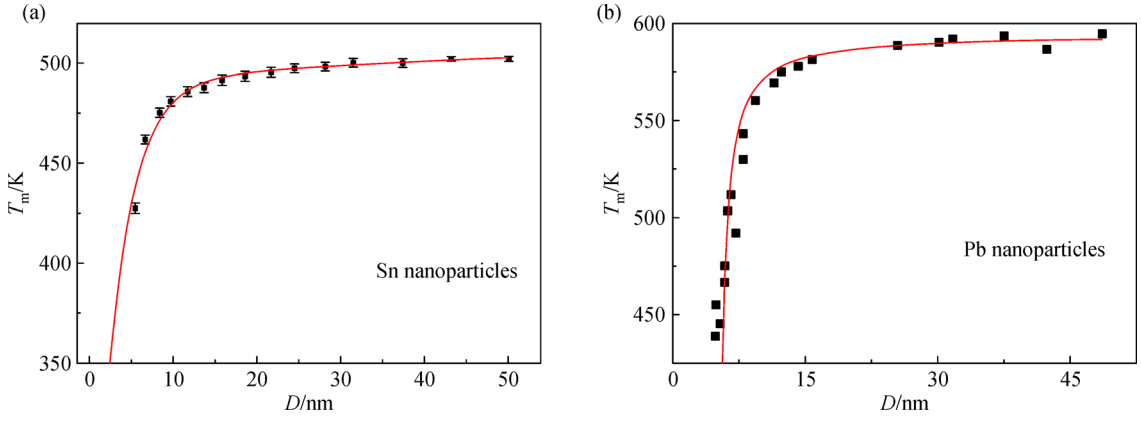

Fig. 12 Comparison of the theory and experiment for Sn and Pb nanoparticles (adapted with permission from Ref. [110]).

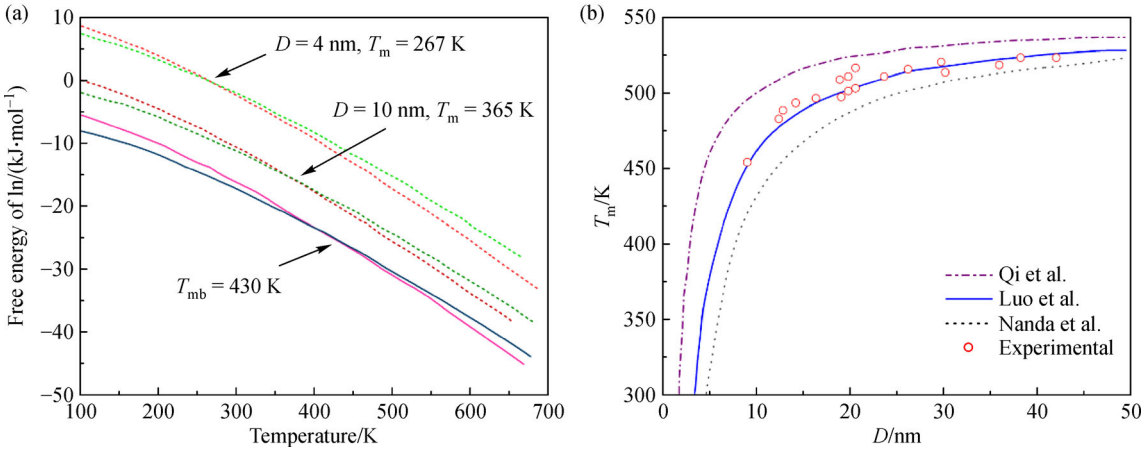

Fig. 13 Effect of binding energy and size on the melting point of nanoparticles (adapted with permission from Ref. [112]). (a) Gibbs free energies of the solid and liquid indium for the bulk material, 10, and 4 nm nanoparticles; (b) comparison of Luo, Qi, and Nada's theory and the experiment of Bi nanoparticle.

Table 5 Molar surface area of different nanosolids [112]

Nanosolid	Molar surface area
Spherical nanoparticles	$A(T) = (6/D)V(T)$
Regular tetrahedral nanoparticles	$A(T) = (6\sqrt{6}/D)V(T)$
Regular icosahedral nanoparticles	$A(T) = [9\sqrt{3}-3\sqrt{15}/D]V(T)$
Cylindrical nanowires	$A(T) = (4/D)V(T)$
Nanofilms	$A(T) = (2/H)V(T)$

Notes: $A(T)$—Molar surface area at temperature T; $V(T)$ —molar volume at temperature T; D and H mean the same as Qi's work.

function of temperature are expressed as follows respectively,

$$V^{\mathrm{l}}(T) = V^{\mathrm{l}}_{\mathrm{m}}[1 + \delta(T - T_{\mathrm{mb}})], \tag{15}$$

$$V^{\mathrm{s}}(T) = \frac{V^{\mathrm{l}}(T)}{1 + \alpha}, \tag{16}$$

where $V^{\mathrm{l}}_{\mathrm{m}}$ is the molar volume of the liquid phase at melting point, δ is the coefficient of thermal expansion of volume, and α is the volume change rate in the melting process, which can be calculated as $\alpha = [V^{\mathrm{l}}_{\mathrm{m}}(T) - V^{\mathrm{s}}_{\mathrm{m}}(T)] / V^{\mathrm{s}}_{\mathrm{m}}(T)$.

The model of Luo et al. takes into account other factors, namely, surface free difference between the solid and liquid phases, the temperature effect on the surface free energy and molar volume, as well as volume change at melting point for nanostructured materials. This theory yields better predictions when interpreting particles such as Bi, In, and Ag than those models of Qi et al.'s and Nanda et al.'s (see Fig. 13(b)).

4.4 Supercooling

The supercooling of gallium is significant, and its temperature can be lowered by orders of magnitude [113]. Gallium-based alloys have a tendency to supercooling since they need more energy for nucleation compared with normal liquids like water. According to the classical theory of nucleation, the energy change of the liquid in the solidification process contains two parts: the difference of volume free energy between the solid-liquid phase ΔG_{p} that is positively correlated with crystallization, and the interface energy σ that is negatively related to crystallization [114]. For a crystal nucleus with a radius r, the total change of the free energy can be calculated as

$$\Delta G_{\mathrm{total}} = -\frac{4}{3}r^3 G_{\mathrm{p}} + 4\pi r^2 \sigma. \tag{17}$$

Figure 14 shows the relationship between the volume free energy, interface energy, and the radius of the crystal nucleus. It can be found that there is a critical radius of the

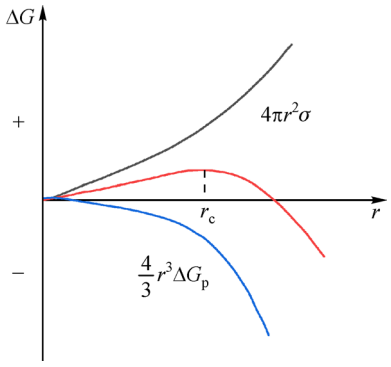

Fig. 14 Relationship between the volume free energy, interface energy and the radius of the crystal.

crystal nucleus below which the crystal nucleus cannot grow spontaneously. The critical radius can be obtained by differentiating the radius of free energy ($\partial \Delta G_{\mathrm{total}}/\partial r = 0$). The critical radius and the critical free energy for nucleation at temperature T can thus be obtained, expressed as Eqs. (18) and (19).

$$r_{\mathrm{c}} = \frac{2\sigma T_{\mathrm{m}}}{\Delta H_{\mathrm{P}}} \cdot \frac{1}{T_{\mathrm{m}} - T}, \tag{18}$$

$$\Delta G_{\mathrm{c}} = \frac{16}{3}\frac{\pi\sigma^3}{\Delta G_{\mathrm{P}}{}^2} = \frac{16\pi\sigma^3 T_{\mathrm{m}}{}^2}{3\Delta H_{\mathrm{P}}{}^2}\frac{1}{(T_{\mathrm{m}} - T)^2}, \tag{19}$$

where T_{m} is the melting point and ΔH_{p} is the volume fusion enthalpy.

In the solidification process, the atoms or molecules in liquids form embryos with the present of thermal motion, and only the embryos with the larger radii r_{c} can be the nucleation centers. Therefore, the critical radius and the critical free energy for nucleation indicate the difficulty of nucleation, and the liquid with a larger r_{c} or ΔG_{c} is more different to form crystal nucleus and more likely to be supercooled. Table 6 lists the thermodynamic parameters of some typical liquids, such as gallium, mercury, bismuth, and water. Based on those parameters, the critical radius and the critical free energy at different temperatures can be calculated, as shown in Figs. 15(a) and 15(b). The calculation shows that bismuth has a larger critical radius and critical free energy than those of other substances, thus pure bismuth droplets should be more easily to be supercooled. The maximum supercooling measured by the experiment are listed in Table 6, which is in agreement with this review.

5 Applications based on melting process of liquid metal

The previous sections demonstrated the fundamental theories and typical effects on the melting point. Through

Table 6 Thermodynamic parameters of typical liquids [100]

Liquid	T_m/K	$\sigma/(10^{-3}\mathrm{J\cdot m^{-2}})$	$\Delta H_f/(10^3\mathrm{J\cdot kg^{-1}})$	$\rho/(10^3\mathrm{kg\cdot m^{-3}})$	ΔT_{max}/K
Gallium	303	55.9	80.00	5.92	76.00
Mercury	234.3	24.4	11.42	13.534	58.00
Bismuth	544	54.4	54.07	10.05	90.00
Water	273.2	32.1	334.00	0.9167	25.00

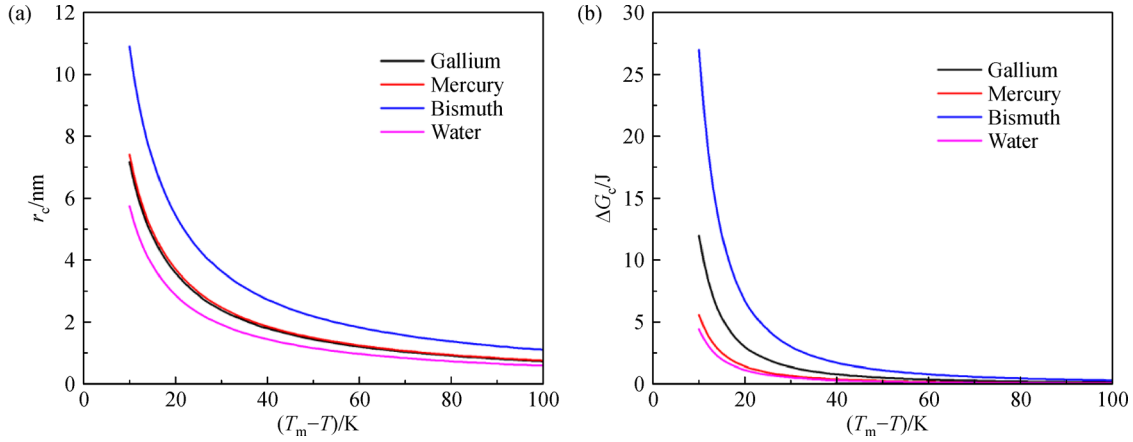

Fig. 15 Critical parameters for nucleation of typical liquids at different temperatures. (a) Critical radius r_c; (b) critical free energy ΔG_c.

these contents, the melting point of liquid metal sample can be calculated when the parameters like structures and the component contents are known. Further, the melting point of liquid meal can be changed by changing the components, the working pressure, and the particle sizes. This will provide a guideline for material designing, which is helpful to the applications. Herein, to illustrate practical applications of liquid metal, several practical examples in the field of the metallic PCMs, heat transfer fluids, and addictive manufacturing are introduced.

5.1 Metallic PCMs

Phase change material (PCM) refers to the substance with a high heat of fusion, which is competent to store or release a huge amount of thermal energy with melting or solidifying. In the melting process, the PCM can absorb a considerable amount of heat energy from the surroundings with its temperature remaining constant or variation in a small range and vice versa in solidification.

Due to the advantages of compact structure, high energy density and convenience for use, the PCM is becoming a promising candidate for more possible thermal applications such as heat storage, temperature control, and so on, the research for which has been a popular topic in the field of heat transfer. Additionally, the PCM can also be a passive cooler for heat impulses in electronics working intermittently, the frequent temperature undulation of these apparatuses being considered. Common PCMs can be divided into three categories based on different chemical compositions, namely organic PCMs, inorganic PCMs, and metallic PCMs (Figs. 16(a)–16(c)).

The process of phase change completely determines the thermal performance of PCM. The most important three thermal parameters are the melting point T_m, which determines the temperature area applied; the thermal conductivity k, which influences the efficiency of heat transfer in the phase change; and enthalpy of fusion ΔH, which represents the ability of heat storage. Compared with metallic PCMs, the inferior conductivity of organic/inorganic PCMs notably limits the efficiencies of heat transfer, thus hindering a better thermal performance. Figure 16(d) clearly shows the distribution of melting point of different PCMs, by which the temperature range of application for a certain PCM is determined [115]. Although the specific enthalpy of fusion of metallic PCMs is lower than that of nonmetallic PCMs (Fig. 16(e)), those metallic ones are better as far as volumetric enthalpy of fusion is concerned (Fig. 16(f)), which enables more applications in an extremely narrow space.

As the metallic PCMs are widely used, Table 7 summarizes the physical properties of their thermal parameters [115]. Ge et al. [6] thoroughly proposed the method of heat control/storage based on liquid metal as a new kind of PCM in 2012, which opened a new heat management mode for electronics devices. Considering the thermal properties, convenience, stability, and cost-efficiency, liquid metals almost represent excellent performances as PCMs, as shown in Fig. 17. Additionally, liquid metals have extremely low melting point as around the

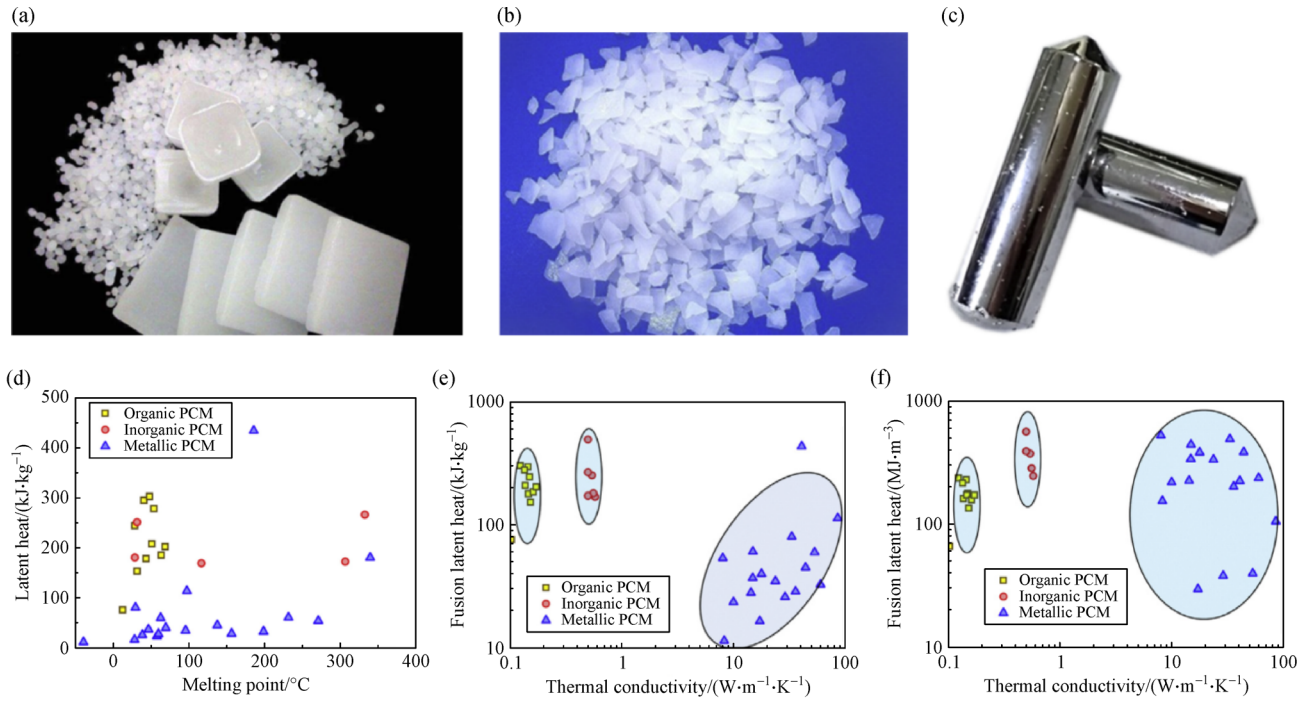

Fig. 16 Examples and property contrast of three common types of PCMs (adapted with permission from Ref. [115]).
(a) Paraffin (organic PCMs); (b) typical hydrated salt ($MgCl_2 \cdot H_2O$, inorganic PCMs); (c) E-BiInSn (low-melting-point metallic PCMs); (d) enthalpy of fusion versus melting point of different PCMs; (e) specific latent heat versus thermal conductivity of different PCMs; (f) volumetric enthalpy of fusion versus thermal conductivity of different PCMs.

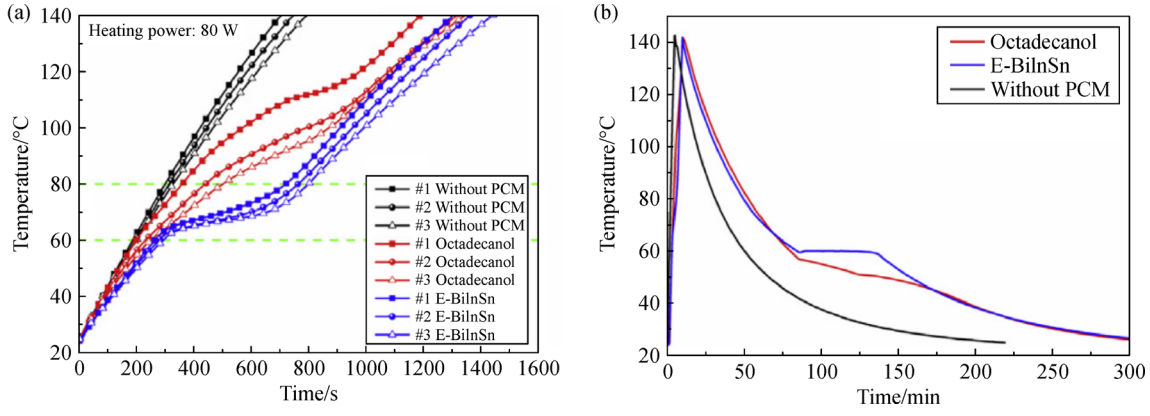

Fig. 17 Temperature responses of different thermal materials.
(a) During heating; (b) natural cooling processes (adapted with permission from Ref. [115]).

room temperature, which can be a promising alternative to replace those nonmetallic PCMs for better thermal management [116,117].

As mentioned above, the liquid metal has a big potential as the PCM, the melting point of which determines the certain temperature range it can be employed. Consequently, the capacity of predicting the melting point of the alloy can help quickly evaluate its properties as PCM. Moreover, as a fateful parameter, the devisable melting temperature can attribute to inventing new alloys to meet different demands. Various choices of liquid metal PCMs (LMPCMs), which are more targeted and precise for thermal management can be obtained by these means.

5.2 Heat transfer fluids

The precise design of the melting point of liquid metals is also quite important for the field of heat transfer. For extreme conditions of high heat flux density such as chip, laser, reactor cooling, etc., it is difficult for traditional heat transfer fluids to meet the existing cooling requirements, and thermal barriers have become the primary problem

Table 7 Comparison of thermal parameters of different metallic PCMs [115]

Metallic PCMs	Melting point T_m/°C	Enthalpy of fusion ΔH/(kJ·kg^{-1})	Density ρ/(kg·m^{-3})	Specific heat capacity c_p/(J·kg^{-1}·°C^{-1})	Thermal conductivity k/(W·m^{-1}·°C^{-1})
Hg	−38.87	11.4	13546(l)	0.139(l)	8.34(l)
Cs	28.65	16.4	1796(l)	0.236(l)	17.4(l)
Ga [94]	29.78	80.16	5904(s)/6095(l)	372.3(s)/397.6(l)	33.49(s)/33.68(l)
Rb	38.85	25.74	1470	0.363	29.3
$Bi_{44.7}Pb_{22.6}In_{19.1}Sn_{8.3}Cd_{5.3}$	47	36.8	9160	0.197	15
$Bi_{49}In_{21}Pb_{18}Sn_{12}$[118]	58.2	23.4	9307(s)	0.213(s)/0.211(l)	7.143(s)/10.1(l)
$Bi_{31.6}In_{48.8}Sn_{19.6}$[119]	60.2	27.9	8043	0.270(s)/0.297(l)	19.2(s)/14.5(l)
K	63.2	59.59	664	0.78	54
$Bi_{50}Pb_{26.7}Sn_{13.3}Cd_{10}$	70	39.8	9580	0.184	18
$Bi_{52}Pb_{30}Sn_{18}$	96	34.7	9600	0.167	24
Na	97.83	113.23	926.9(l)	1.38(l)	86.9(l)
$Bi_{58}Sn_{42}$	138	44.8	8560	0.201	44.8
In	156.8	28.59	7030	0.23(l)	36.4(l)
Li	186	433.78	515(l)	4.389(l)	41.3
$Sn_{91}Zn_9$	199	32.5	7270	0.272	61
Sn	232	60.5	7300(s)	0.221	15.08(s)
Bi	271.4	53.5	9790	0.122	8.1
$Zn_{52}Mg_{48}$	340	180	—	—	—
$Al_{59}Mg_{35}Zn_6$	443	310	2380	1.63(s)/1.46(l)	—
$Al_{65}Cu_{30}Si_5$	571	422	2730	1.3(s)/1.2(l)	—
$Zn_{49}Cu_{45}Mg_6$	703	176	8670	0.42(s)	—
$Cu_{80}Si_{20}$	803	197	6600	0.5(s)	—
$Si_{56}Mg_{44}$	946	757	1900	0.79(s)	—

Notes: l—Liquid phase; s—solid phase.

limiting their development. Liquid metal and its alloys, due to its high thermal conductivity and flow characteristics, have outstanding performances in these advanced heat exchange fields. In 2002, Liu's team first proposed the use of liquid metal as a heat transfer medium to efficiently cool the chip [120]. Since then, they have conducted a series of theoretical analyses, experimental testing, numerical simulation, and optimization design for liquid metal cooling systems [31,47,121–123].

Clearly, if the working fluid with low-melting point can be obtained by the precise design method, the heat exchange temperature range of the liquid metal could be broadened. In this way, liquid metal, which has a high efficiency in the heat exchange filed, can be applied to more areas. For example, liquid metals can be used to recover industrial low-grade waste heat. The low-grade heat is the part of the heat that is left in industrial production and cannot continue to work for industry. The liquid metal with an efficient heat transfer has the potential in this field application by choosing a suitable flowing temperature.

5.3 Addictive manufacturing

Flexible electronics have attracted the interests in customization and industrialization owing to its intrinsic security and portability of design [124–134]. With the advancement of printing technology, the needs for complex shapes and multifunctional print patterns have been increasing. However, the printing consumables currently used are polymers, which are insulative and non-transformable. For traditional metal printing materials, the powdered metal is first melted by a high-temperature probe, and then reshaped to obtain a corresponding printed shape. This method that demanded a high operating temperature and pivotal performance of the probe, cannot be widely promoted in the consumer electronics industry. Recently, because of high price and complicated preparation processes (sputtering, spin coating, etc.), the applications of precious metal pastes (such as gold and silver paste) are confining except of the fabrication of precision instruments [128,135]. Room temperature liquid metal is an excellent 3D printing ink consumable due to its

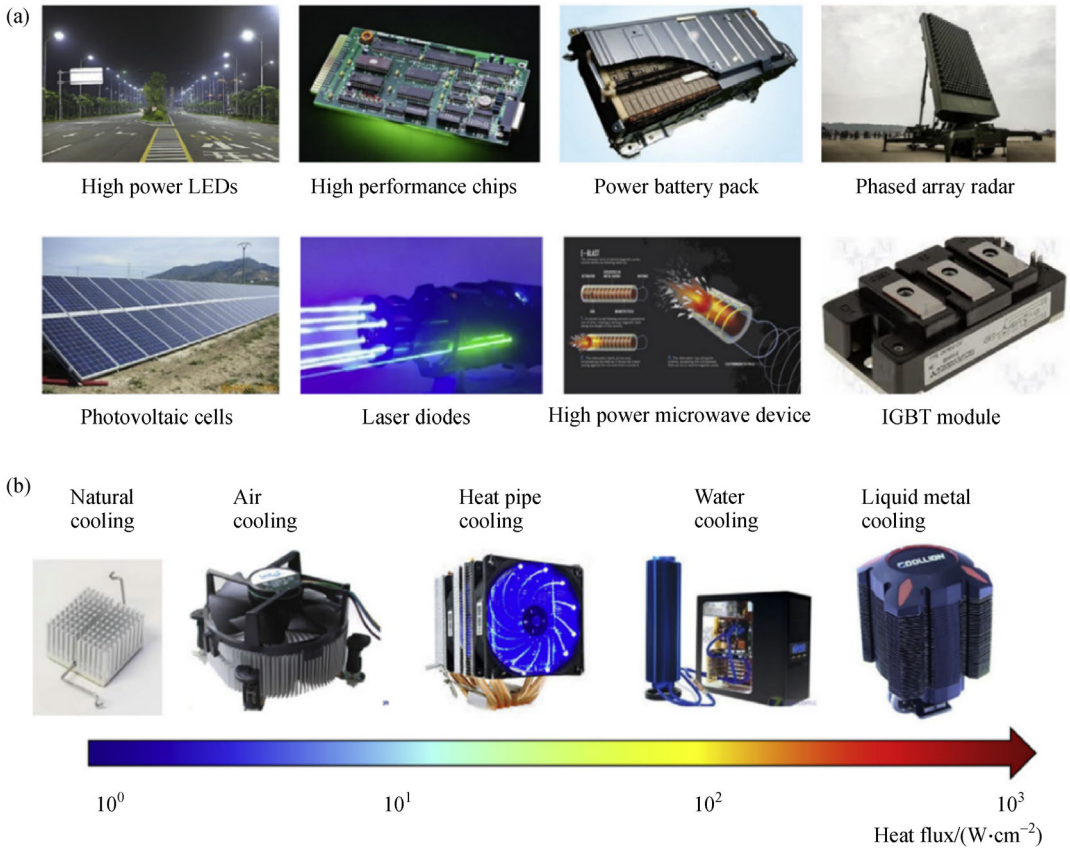

Fig. 18 High density heat production equipment and heat transfer efficiency (adapted with permission from Ref. [115]). (a) Devices and components with high heat generation; (b) development of commercial chip-cooling technologies.

rheology and good electrical and thermal conductivity [136]. The low-melting liquid metal ink interacts well with non-metallic materials in the manufacturing process, realizing rapid low-cost prototyping of various electronic circuit functional devices, and avoiding the etching process of conventional printing.

Zheng et al. [137] proposed and demonstrated the printer machine that can directly print ductile electronics on paper with a low melting-point liquid metal at room temperature. Hereafter, the realization of direct printing technology on different substrates becomes a research hotspot owing to the large surface tension and non-wetting property of the liquid metal [138–141].

It is a core issue to formulate liquid metal inks with suitable melting points to meet different working conditions. When metal gallium with other different kinds of metals are alloyed at different contents, the melting process and the external energy required are diverging, which would eventually affect the performance of the final substance. The exploration of the melting process of different metals would contribute to obtaining suitable printing inks for different substrates. This improved method not only is material saving, cost-effective, but also controls the alloying process very well, making the reaction safer and more tunable.

6 Summary and outlook

It is important to fully understand the fundamental theories and factors that influence the melting point of liquid metals. Besides, such efforts are imperative for material design and industrial applications. In this paper, the theory for calculating the melting point of substances have been summarized, including the thermodynamics based on Gibbs free energy and the molecular dynamics simulations based on the atomic interactions. After that, some typical factors that have specific effects on the melting point of liquid metal, such as composition, pressure, and size, have been discussed in detail. Then, some practical applications with liquid metals have been illustrated.

To create more types of low melting point alloys and broaden practical applications such as in the field of elastic electronics, bio-engineering and flexible robotics, the following points should be further analyzed and discussed.

(1) Crystal nucleation process at microscale. The melting point of a metal is related to the size of its particles, and there are also magic numbers in the cluster [77]. The criterions derived from different physicochemical methods are related to the unit cell structure and thermal motion. Currently, only simple crystal metals can be analyzed [52,58,142–144]. Therefore, from the struc-

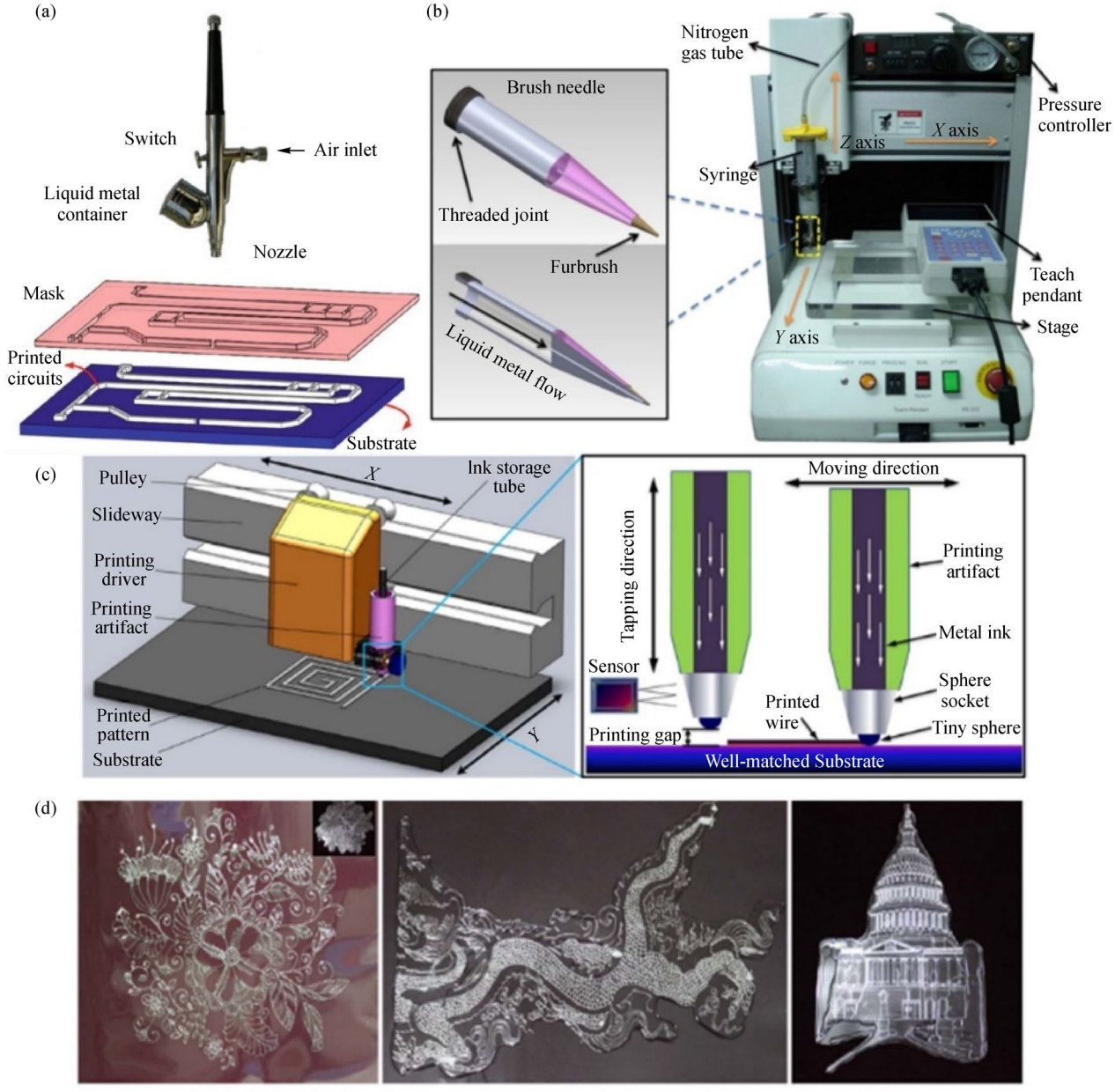

Fig. 19 Different printing methods and printed patterns.
(a) Mask printing technology (adapted with permission from Refs. [26,138]); (b) direct desktop printing method (adapted with permission from Refs. [26,137]); (c) scheme of low-cost computer-controlled printer; (d) directly printed and packaged pattern (adapted with permission from Refs. [26,139]).

ture of the unit cell and the band theory, it is still necessary to conduct more basic investigations on the composition and function of the low melting point alloy.

(2) The melting mechanism of the alloy. The melting process derived from the relationship between Gibbs free energy is only effective in low-element alloys. Due to the assumption and simplification of the prediction of the melting process of multi-alloys, the solution of melting point about low-melting multi-alloys is still a challenge.

(3) Numerical simulation of low melting point alloys. Considering the computational power, the existing molecular dynamics methods can only calculate the few atoms or atom clusters whose number of metal atoms in the molecular simulation process is far away from the composition of the macroscale metal. Furthermore, the liquid metal has a degree of subcooling. Therefore, it still poses a challenge to accurately obtain the overall melting point with the suitable molecular weight selection. At present, since the constituent elements of the low melting point alloy are mostly complex crystal metals, molecular dynamics simulation calculations of the liquid metal have not yet been studied. Therefore, the theoretical calculation

of the melting point data of various proportioning alloys, and the better adjustment of the liquid metal to meet the working requirements experimentally, are important issues in the work to be followed next.

(4) Design of functional composites. The addition of nanoparticles and polymer materials to the low-melting alloy to obtain the desired reinforcing properties or special properties, such as magnetic properties, photoelectric conversion properties, etc., plays an important role in realizing the application technology of the low-melting alloy. Many attempts have been made to combine the flexible substrate with the enhanced electrical and thermal conductivity. Therefore, the use of the high surface tension of the liquid metal to perform composite crossover on flexible machines and smart materials is still worth considering.

In summary, the low melting-point liquid metal with commendable merits, especially its rheological behaviors and metallic properties, would bring widespread potential applications in emerging frontiers including flexible electronics, soft robotics, and advanced thermal management. Mastering the basic physical properties of materials not only helps design materials, but also develops many cutting edge applications via their unique material properties. In the near future, in order to extend the research categories of liquid metal, theoretical and experimental approaches should provide an important avenue for mastering the intrinsic characteristics of fusion among liquid metals.

Acknowledgements This work was partially supported by the National Natural Science Foundation of China under Key Project (Grant No. 91748206), Dean's Research Funding of the Chinese Academy of Sciences, and the Frontier Project of the Chinese Academy of Sciences.

References

1. Gough R C, Morishita A M, Dang J H, Moorefield M R, Shiroma W A, Ohta A T. Rapid electrocapillary deformation of liquid metal with reversible shape retention. Micro & Nano Systems Letters, 2015, 3(1): 4
2. Jin C, Zhang J, Li X, Yang X, Li J, Liu J. Injectable 3-D fabrication of medical electronics at the target biological tissues. Scientific Reports, 2013, 3(1): 3442
3. Liang S, Rao W, Song K, Liu J. Fluorescent liquid metal as transformable biomimetic chameleon. ACS Applied Materials & Interfaces, 2018, 10(2): 1589–1596
4. Sen P, Kim C J. Microscale liquid-metal switches—a review. IEEE Transactions on Industrial Electronics, 2009, 56(4): 1314–1330
5. Prokhorenko V Y, Roshchupkin V V, Pokrasin M A, Prokhorenko S V, Kotov V V. Liquid gallium: potential uses as a heat-transfer agent. High Temperature, 2000, 38(6): 954–968
6. Ge H, Li H, Mei S, Liu J. Low melting point liquid metal as a new class of phase change material: an emerging frontier in energy area. Renewable & Sustainable Energy Reviews, 2013, 21: 331–346
7. Liu J, Zhou Y X, Lv Y G, Li T. Liquid metal based miniaturized chip-cooling device driven by electromagnetic pump. In: ASME 2005 International Mechanical Engineering Congress and Exposition, 2005, (42177): 501–510
8. Ge H, Liu J. Phase change effect of low melting point metal for an automatic cooling of USB flash memory. Frontiers in Energy, 2012, 6(3): 207–209
9. Ge H, Liu J. Keeping smartphones cool with gallium phase change material. Journal of Heat Transfer, 2013, 135(5): 054503
10. Yan J, Lu Y, Chen G, Yang M, Gu Z. Advances in liquid metals for biomedical applications. Chemical Society Reviews, 2018, 47(8): 2518–2533
11. Yi L, Ding Y, Yuan B, Wang L, Tian L, Chen C, Liu F, Lu J, Song S, Liu J. Breathing to harvest energy as a mechanism towards making a liquid metal beating heart. RSC Advances, 2016, 6(97): 94692–94698
12. Yi L, Jin C, Wang L, Liu J. Liquid-solid phase transition alloy as reversible and rapid molding bone cement. Biomaterials, 2014, 35 (37): 9789–9801
13. Sun X, Sun M, Liu M, Yuan B, Gao W, Rao W, Liu J. Shape tunable gallium nanorods mediated tumor enhanced ablation through near-infrared photothermal therapy. Nanoscale, 2019, 11 (6): 2655–2667
14. Khoshmanesh K, Tang S Y, Zhu J Y, Schaefer S, Mitchell A, Kalantar-zadeh K, Dickey M D. Liquid metal enabled microfluidics. Lab on a Chip, 2017, 17(6): 974–993
15. Maddaluno G, Marzullo D, Mazzitelli G, Roccella S, Di Gironimo G, Zanino R. The DTT device: divertor solutions for alternative configurations including liquid metals. Fusion Engineering and Design, 2017, 122: 341–348
16. Gao M, Gui L. Development of a fast thermal response microfluidic system using liquid metal. Journal of Micromechanics and Microengineering, 2016, 26(7): 075005
17. Han B, Yang Y, Shi X B, Zhang G, Gong L, Xu D, Zeng H, Wang C, Gu M, Deng Y. Spontaneous repairing liquid metal/Si nanocomposite as a smart conductive-additive-free anode for lithium-ion battery. Nano Energy, 2018, 50: 359–366
18. Liu G, Kim J Y, Wang M, Woo J Y, Wang L, Zou D, Lee J K. Soft, highly elastic, and discharge-current-controllable eutectic gallium-indium liquid metal-air battery operated at room temperature. Advanced Energy Materials, 2018, 8(16): 1703652
19. Wu J, Tang S Y, Fang T, Li W, Li X, Zhang S. A wheeled robot driven by a liquid-metal droplet. Advanced Materials, 2018, 30 (51): 1805039
20. Yao Y Y, Liu J. Liquid metal wheeled small vehicle for cargo delivery. RSC Advances, 2016, 6(61): 56482–56488
21. Wang D L, Gao C Y, Wang W, Sun M, Guo B, Xie H, He Q. Shape-transformable, fusible rodlike swimming liquid metal nanomachine. ACS Nano, 2018, 12(10): 10212–10220
22. Chen S, Yang X, Cui Y, Liu J. Self-growing and serpentine locomotion of liquid metal induced by copper ions. ACS Applied Materials & Interfaces, 2018, 10(27): 22889–22895
23. Zeng M Q, Fu L. Controllable fabrication of graphene and related two-dimensional materials on liquid metals via chemical vapor deposition. Accounts of Chemical Research, 2018, 51(11): 2839–2847
24. Liang S T, Wang H Z, Liu J. Progress, mechanisms and

applications of liquid-metal catalyst systems. Chemistry, 2018, 24 (67): 17616–17626
25. Zavabeti A, Zhang B Y, de Castro I A, Ou J Z, Carey B J, Mohiuddin M, Datta R, Xu C, Mouritz A P, McConville C F, O'Mullane A P, Daeneke T, Kalantar‐Zadeh K. Green synthesis of low-dimensional aluminum oxide hydroxide and oxide using liquid metal reaction media: ultrahigh flux membranes. Advanced Functional Materials, 2018, 28 (44): 1804057(9)
26. Wang Q, Yu Y, Liu J. Preparations, characteristics and applications of the functional liquid metal materials. Advanced Engineering Materials, 2017, 20(5): 1700781
27. Guo R, Tang J, Dong S, Lin J, Wang H, Liu J, Rao W. One-step liquid metal transfer printing: toward fabrication of flexible electronics on wide range of substrates. Advanced Materials Technologies, 2018, 3(12): 1800265(13)
28. Van Meerbeek I M, Mac Murray B C, Kim J W, Robinson S S, Zou P X, Silberstein M N, Shepherd R F. Morphing metal and elastomer bicontinuous foams for reversible stiffness, shape memory, and self-healing soft machines. Advanced Materials, 2016, 28(14): 2801–2806
29. Wada T, Geslin P A, Kato H. Preparation of hierarchical porous metals by two-step liquid metal dealloying. Scripta Materialia, 2018, 142: 101–105
30. Wang H, Yuan B, Liang S, Guo R, Rao W, Wang X, Chang H, Ding Y, Liu J, Wang L. Plus-M: a porous liquid-metal enabled ubiquitous soft material. Materials Horizons, 2018, 5(2): 222–229
31. Ma K Q, Liu J. Nano liquid-metal fluid as ultimate coolant. Physics Letters. [Part A], 2007, 361(3): 252–256
32. Zhao X, Tang J, Yu Y, Liu J. Transformable soft quantum device based on liquid metals with sandwiched liquid junctions. arXiv e-prints [Online], 2017:1710.09098
33. Tang J, Zhao X, Li J, Zhou Y, Liu J. Liquid metal phagocytosis: intermetallic wetting induced particle internalization. Advancement of Science, 2017, 4(5): 1700024
34. Tien C, Wur C, Lin K, Charnaya E V, Kumzerov Y A. Freezing and melting of gallium in porous glass. Solid State Communications, 1997, 104(12): 753–757
35. Daeneke T, Khoshmanesh K, Mahmood N, de Castro I A, Esrafilzadeh D, Barrow S J, Dickey M D, Kalantar-zadeh K. Liquid metals: fundamentals and applications in chemistry. Chemical Society Reviews, 2018, 47(11): 4073–4111
36. Markvicka E J, Bartlett M D, Huang X, Majidi C. An autonomously electrically self-healing liquid metal-elastomer composite for robust soft-matter robotics and electronics. Nature Materials, 2018, 17(7): 618–624
37. Li X K, Li M J, Zong L, Wu X, You J, Du P, Li C. Liquid metal droplets wrapped with polysaccharide microgel as biocompatible aqueous ink for flexible conductive devices. Advanced Functional Materials, 2018, 28 (39): 1804197 (8)
38. Lin Y, Genzer J, Li W, Qiao R, Dickey M D, Tang S Y. Sonication-enabled rapid production of stable liquid metal nanoparticles grafted with poly(1-octadecene-alt-maleic anhydride) in aqueous solutions. Nanoscale, 2018, 10(42): 19871–19878
39. Park S, Thangavel G, Parida K, Li S, Lee P S. A stretchable and self-healing energy storage device based on mechanically and electrically restorative liquid-metal particles and carboxylated polyurethane composites. Advanced Materials, 2019, 31(1): 1805536
40. Miracle D B, Senkov O N. A critical review of high entropy alloys and related concepts. Acta Materialia, 2017, 122: 448–511
41. Lei Z, Liu X, Wu Y, Wang H, Jiang S, Wang S, Hui X, Wu Y, Gault B, Kontis P, Raabe D, Gu L, Zhang Q, Chen H, Wang H, Liu J, An K, Zeng Q, Nieh T G, Lu Z. Enhanced strength and ductility in a high-entropy alloy via ordered oxygen complexes. Nature, 2018, 563(7732): 546–550
42. Tang S Y, Qiao R, Yan S, Yuan D, Zhao Q, Yun G, Davis T P, Li W. Microfluidic mass production of stabilized and stealthy liquid metal nanoparticles. Small, 2018, 14(21): 1800118
43. Chu K, Song B G, Yang H I, Kim D M, Lee C S, Park M, Chung C M. Smart passivation materials with a liquid metal microcapsule as self-healing conductors for sustainable and flexible perovskite solar cells. Advanced Functional Materials, 2018, 28(22): 1800110
44. Tan L, Zeng M, Zhang T, Fu L. Design of catalytic substrates for uniform graphene films: from solid-metal to liquid-metal. Nanoscale, 2015, 7(20): 9105–9121
45. Wang J, Zeng M, Tan L, Dai B, Deng Y, Rümmeli M, Xu H, Li Z, Wang S, Peng L, Eckert J, Fu L. High-mobility graphene on liquid p-block elements by ultra-low-loss CVD growth. Scientific Reports, 2013, 3(1): 2670
46. Sun N, He X, Dong K, Zhang X, Lu X, He H, Zhang S. Prediction of the melting points for two kinds of room temperature ionic liquids. Fluid Phase Equilibria, 2006, 246(1–2): 137–142
47. Ma K, Liu J. Liquid metal cooling in thermal management of computer chips. Frontiers of Energy and Power Engineering in China, 2007, 1(4): 384–402
48. Wang L, Liu J. Liquid metal material genome: Initiation of a new research track towards discovery of advanced energy materials. Frontiers in Energy, 2013, 7(3): 317–332
49. Zhou K, Tang Z, Lu Y, Wang T, Wang H, Li T. Composition, microstructure, phase constitution and fundamental physicochemical properties of low-melting-point multi-component eutectic alloys. Journal of Materials Science and Technology, 2017, 33(2): 131–154
50. Lindemann F A. The calculation of molecular vibration frequencies. Physikalische Zeitschrift, 1910, 11: 609–612
51. Zhang S, Zhang W. The generalized Lindemann melting law. Chinese Journal of Computational Physics, 1985, 2(1): 91–98
52. Bedoya-Martínez O N, Kaczmarski M, Hernández E R. Melting temperature of fcc metals using empirical potentials. Journal of Physics Condensed Matter, 2006, 18(34): 8049–8062
53. Cahn R W. Melting from within. Nature, 2001, 413(6856): 582–583
54. Gupta N P. On the Lindemann law of melting of solids. Solid State Communications, 1973, 13(1): 69–71
55. Goldman V V. Debye-waller factors in rare-gas solids. Physical Review, 1968, 174(3): 1041–1045
56. Guinea F, Rose J H, Smith J R, Ferrante J. Scaling relations in the equation of state, thermal expansion, and melting of metals. Applied Physics Letters, 1984, 44(1): 53–55
57. Born M. Thermodynamics of crystals and melting. Journal of Chemical Physics, 1939, 7(8): 591–603
58. Shibuta Y, Suzuki T. Melting and solidification point of fcc-metal

nanoparticles with respect to particle size: a molecular dynamics study. Chemical Physics Letters, 2010, 498(4–6): 323–327
59. Yang L, Gan X, Xu C, Lang L, Jian Z, Xiao S, Deng H, Li X, Tian Z, Hu W. Molecular dynamics simulation of alloying during sintering of Li and Pb metallic nanoparticles. Computational Materials Science, 2019, 156: 47–55
60. Birchenall C E, Riechman A F. Heat storage in eutectic alloys. Metallurgical Transactions. A, Physical Metallurgy and Materials Science, 1980, 11(8): 1415–1420
61. Farkas D, Birchenall C E. New eutectic alloys and their heats of transformation. Metallurgical Transactions A, Physical Metallurgy and Materials Science, 1985, 16(3): 323–328
62. Fu X, Shen W, Yao T, Hou W. Physical Chemistry. 5th ed. Beijing: Higher Education Press, 2015 (in Chinese)
63. Pan A, Wang J, Zhang X. Prediction of melting temperature and latent heat for low-melting metal PCMs. Rare Metal Materials and Engineering, 2016, 45(4): 874–880
64. Laar J J V, Schmelzoder D. Erstarrungskurven bei binären Systemen, wenn die feste Phase ein Gemisch (amorphe feste Lösung oder Mischkristalle) der beiden Komponenten ist. Zeitschrift für Physikalische Chemie, 1908, 63U(1): 216
65. Wang L. Theoretical and experimental studies on liquid metal functional materials for additive manufacturing. Dissertation for the Doctoral Degree. Beijing: University of Chinese Academy of Science, 2015 (in Chinese)
66. Qiao Z, Xu Z, Liu H. Metallurgy and Materials Calculation Physical Chemistry. Beijing: Metallurgical Industry Press, 1999 (in Chinese)
67. Xu Z. Material Thermodynamics. Beijing: Higher Education Press, 2009 (in Chinese)
68. Li Y W, Chang K K, Wang P S, Hu B, Zhang L J, Liu S H, Du Y. Calculation of phase diagram and its application. Materials Science Engineering of Powder Metallurgy, 2012, 17(1): 1–9
69. Easterling K E, Porter D A. S Mohamed Y. Phase Transformations in Metals and Alloys. 3rd ed. CRC Press, 2009
70. Wen Y, Zhu R, Zhou F, et al. An overview on molecular dynamics simulation. Advances in Mechanics, 2003, 33(1): 65–73
71. Daw M S, Baskes M I. Embedded-atom method: derivation and application to impurities, surfaces, and other defects in metals. Physical Review B, 1984, 29(12): 6443–6453
72. Etesami S A, Asadi E. Molecular dynamics for near melting temperatures simulations of metals using modified embedded-atom method. Journal of Physics and Chemistry of Solids, 2018, 112: 61–72
73. Asadi E, Asle Zaeem M, Nouranian S, Baskes M I. Two-phase solid–liquid coexistence of Ni, Cu, and Al by molecular dynamics simulations using the modified embedded-atom method. Acta Materialia, 2015, 86: 169–181
74. Wilhelm R M. Freezing point of mercury. Scientific Papers of the Bureau of Standards, 1916, 13
75. Greenwood N N, Earnshaw A. Chemistry of the Elements. 2nd ed. Oxford: Pergamon Press, 1984
76. Norrby L J. Why is mercury liquid? Or, why do relativistic effects not get into chemistry textbooks? Journal of Chemical Education, 1991, 68(2): 110–113
77. Calvo F, Pahl E, Wormit M, Schwerdtfeger P. Evidence for low-temperature melting of mercury owing to relativity. Angewandte Chemie International Edition, 2013, 52(29): 7583–7585
78. Abbaschian G J, Ravitz S F. Melting kinetics of gallium single crystals. Journal of Crystal Growth, 1975, 28(1): 16–20
79. Bartis F J. The soft modes of melting. Physics Letters. [Part A], 2004, 333(5–6): 433–437
80. Jach J, Sebba F. The melting of gallium. Transactions of the Faraday Society, 1954, 50: 226–231
81. Boedtker O A, Force R C L, Kendall W B, Ravitz S F. Melting of gallium. Transactions of the Faraday Society, 1965, 61: 665–667
82. Bridgman P W. Polymorphism, principally of the elements, up to 50000 kg/cm^2. Physical Review, 1935, 48(11): 893–906
83. Gong X. Eletronic structures on solid gallium. Acta Physica Sinica, 1993, 42(4): 617–625 (in Chinese)
84. Gong X. Ab-inition molecular dynamics studies on gallium clusters. Acta Physica Sinica, 1993, 42(2): 244–251 (in Chinese)
85. Bernasconi M, Chiarotti G L, Tosatti E. Ab initio calculations of structural and electronic properties of gallium solid-state phases. Physical Review. B, 1995, 52(14): 9988–9998
86. Barman S R, Sarma D D. Electronic structures of gallium and indium across the solid-liquid transition. Physical Review. B, 1995, 51(7): 4007–4013
87. Hakvoort G, van Reijen L L, Aartsen A J. Measurement of the thermal conductivity of solid substances by DSC. Thermochimica Acta, 1985, 93: 317–320
88. Shaker R E, Brantley W A, Wu Q, Culbertson B M. Use of DSC for study of the complex setting reaction and microstructural stability of a gallium-based dental alloy. Thermochimica Acta, 2001, 367–368: 393–400
89. He H, Fei G T, Cui P, Zheng K, Liang L M, Li Y, De Zhang L. Relation between size and phase structure of gallium: differential scanning calorimeter experiments. Physical Review. B, 2005, 72 (7): 073310–073313
90. Kumar V B, Porat Z E, Gedanken A. DSC measurements of the thermal properties of gallium particles in the micron and sub-micron sizes, obtained by sonication of molten gallium. Journal of Thermal Analysis and Calorimetry, 2015, 119(3): 1587–1592
91. Chen S, Wang L, Liu J. Softening theory of matter tuning atomic border to make soft materials. arXiv e-prints [Online], 2018: 1804.01340
92. Ben-David O, Levy A, Mikhailovich B, Azulay A. Impact of rotating permanent magnets on gallium melting in an orthogonal container. International Journal of Heat and Mass Transfer, 2015, 81: 373–382
93. Ben-David O, Levy A, Mikhailovich B, Azulay A. 3D numerical and experimental study of gallium melting in a rectangular container. International Journal of Heat and Mass Transfer, 2013, 67: 260–271
94. Yang X H, Tan S C, Liu J. Numerical investigation of the phase change process of low melting point metal. International Journal of Heat and Mass Transfer, 2016, 100: 899–907
95. Yang X H, Liu J. A novel method for determining the melting point, fusion latent heat, specific heat capacity and thermal conductivity of phase change materials. International Journal of Heat and Mass Transfer, 2018, 127: 457–468
96. Wang R H, Ye Y F, Min G H, Teng X Y, Qin J Y. Study on liquid

structure and viscosity of eutectic gallium-indium alloy. Chin Shu Hsueh Pao, 2001, 37(8): 801–804 (in Chinese)
97. Xiao X, Deng Z, Liu J. In differential scanning calorimetric study on phase transformation characteristics of gallium-based alloys. In: China Society of Engineering Thermophysics Conference, Dongguan, 2013, 123687 (in Chinese)
98. Yu Q, Zhang Q, Zong J, Liu S, Wang X, Wang X, Zheng H, Cao Q, Zhang D, Jiang J. Identifying surface structural changes in a newly-developed Ga-based alloy with melting temperature below 10°C. Applied Surface Science, 2019, 492: 143–149
99. Aleksandrov V D, Frolova S A. Effect of the overheating of the gallium melt on its supercooling during solidification. Russian Metallurgy (Metally), 2014, 2014(1): 14–19
100. Turnbull D. Formation of crystal nuclei in liquid metals. Journal of Applied Physics, 1950, 21(10): 1022–1028
101. Xiao X. Differential scanning calorimetric study on phase transformation characteristics of gallium and gallium-based alloys. Dissertation for the Doctoral Degree. Beijing: University of Chinese Academy of Science, 2013 (in Chinese)
102. Beaupere N, Soupremanien U, Zalewski L. Nucleation triggering methods in supercooled phase change materials (PCM), a review. Thermochimica Acta, 2018, 670: 184–201
103. Sandnes B. The physics and the chemistry of the heat pad. American Journal of Physics, 2008, 76(6): 546–550
104. Garai J, Chen J. Pressure effect on the melting temperature. arXiv e-prints [Online], 2009: 0906.3331
105. Jayaraman A, Klement W Jr, Newton R C, Kennedy G C. Fusion curves and polymorphic transitions of the group III elements—aluminum, gallium, indium and thallium—at high pressures. Journal of Physics and Chemistry of Solids, 1963, 24(1): 7–18
106. Bosio L. Crystal structures of Ga(II) and Ga(III). Journal of Chemical Physics, 1978, 68(3): 1221–1223
107. Bernasconi M, Chiarotti G L, Tosatti E. Ab initiocalculations of structural and electronic properties of gallium solid-state phases. Physical Review. B, 1995, 52(14): 9988–9998
108. Gallium (Ga) Crystal Structure. Datasheet from “Pauling File Multinaries Edition–2012” in Springer Materials. 2019–6, available at materials.springer website
109. Zhang M, Yao S, Rao W, Liu J. Transformable soft liquid metal micro/nanomaterials. Materials Science and Engineering Reports, 2019, 138: 1–35
110. Qi W H. Size effect on melting temperature of nanosolids. Physica B, Condensed Matter, 2005, 368(1–4): 46–50
111. Nanda K K, Sahu S N, Behera S N. Liquid-drop model for the size-dependent melting of low-dimensional systems. Physical Review A., 2002, 66(1): 013208–013215
112. Luo W, Su K, Li K, Li Q. Connection between nanostructured materials’ size-dependent melting and thermodynamic properties of bulk materials. Solid State Communications, 2011, 151(3): 229–233
113. Turnbull D. The subcooling of liquid metals. Journal of Applied Physics, 1949, 20(8): 817
114. Song W. Metallology. Revised ed. Beijing: Metallurgical Industry Press, 1980 (in Chinese)
115. Yang X H, Liu J. Advances in liquid metal science and technology in chip cooling and thermal management. Advances in Heat Transfer, 2018, 50: 187–300
116. Zhang X D, Gao J Y, Zhang P J, Liu J. Comparison on enhanced phase change heat transfer of low melting point metal melting using different heating methods. Journal of Enhanced Heat Transfer, 2019, 26(2): 179–194
117. Zhang X D, Yang X H, Zhou Y X, Rao W, Gao J Y, Ding Y J, Shu Q Q, Liu J. Experimental investigation of galinstan based minichannel cooling for high heat flux and large heat power thermal management. Energy Conversion and Management, 2019, 185: 248–258
118. Fan L W, Wu Y Y, Xiao Y Q, Zeng Y, Zhang Y L, Yu Z T. Transient performance of a thermal energy storage-based heat sink using a liquid metal as the phase change material. Applied Thermal Engineering, 2016, 109: 746–750
119. Yang X H, Tan S C, Ding Y J, Wang L, Liu J, Zhou Y X. Experimental and numerical investigation of low melting point metal based PCM heat sink with internal fins. International Communications in Heat and Mass Transfer, 2017, 87: 118–124
120. Yang X H, Liu J. Advanced liquid metal cooling: historical developments and research frontiers. Science & Technology Review, 2018, 36(15): 54–66
121. Zhang X D, Sun Y, Chen S, Liu J. Unconventional hydrodynamics of hybrid fluid made of liquid metals and aqueous solution under applied fields. Frontiers in Energy, 2018, 12(2): 276–296
122. Miner A, Ghoshal U. Cooling of high-power-density microdevices using liquid metal coolants. Applied Physics Letters, 2004, 85(3): 506–508
123. Tang J, Wang J, Liu J, Zhou Y. A volatile fluid assisted thermo-pneumatic liquid metal energy harvester. Applied Physics Letters, 2016, 108(2): 023903–023906
124. Zhang Z, Cui L, Shi X, Tian X, Wang D, Gu C, Chen E, Cheng X, Xu Y, Hu Y, Zhang J, Zhou L, Fong H H, Ma P, Jiang G, Sun X, Zhang B, Peng H. Textile display for electronic and brain-interfaced communications. Advanced Materials, 2018, 30(18): 1800323
125. Wang J, Tenjimbayashi M, Tokura Y, Park J Y, Kawase K, Li J, Shiratori S. Bionic fish-scale surface structures fabricated via air/water interface for flexible and ultrasensitive pressure sensors. ACS Applied Materials & Interfaces, 2018, 10(36): 30689–30697
126. Xia S, Song S, Gao G. Robust and flexible strain sensors based on dual physically cross-linked double network hydrogels for monitoring human-motion. Chemical Engineering Journal, 2018, 354: 817–824
127. Gao Y, Ota H, Schaler E W, Chen K, Zhao A, Gao W, Fahad H M, Leng Y, Zheng A, Xiong F, Zhang C, Tai L C, Zhao P, Fearing R S, Javey A. Wearable microfluidic diaphragm pressure sensor for health and tactile touch monitoring. Advanced Materials, 2017, 29 (39): 1701985
128. Jeong Y R, Kim J, Xie Z, Xue Y, Won S M, Lee G, Jin S W, Hong S Y, Feng X, Huang Y, Rogers J A, Ha J S. A skin-attachable, stretchable integrated system based on liquid GaInSn for wireless human motion monitoring with multi-site sensing capabilities. NPG Asia Materials, 2017, 9(10): e443
129. Jian M Q, Xia K L, Wang Q, Yin Z, Wang H M, Wang C Y, Xie H H, Zhang M C, Zhang Y Y. Flexible and highly sensitive pressure

sensors based on bionic hierarchical structures. Advanced Functional Materials, 2017, 27(9): 1606066

130. Kim S, Oh J, Jeong D, Park W, Bae J. Consistent and reproducible direct ink writing of eutectic gallium-indium for high-quality soft sensors. Soft Robotics, 2018, 5(5): 601–612
131. Kweon O Y, Lee S J, Oh J H. Wearable high-performance pressure sensors based on three-dimensional electrospun conductive nanofibers. NPG Asia Materials, 2018, 10(6):540–551
132. Jeong Y R, Lee G, Park H, Ha J S. Stretchable, skin-attachable electronics with integrated energy storage devices for biosignal monitoring. Accounts of Chemical Research, 2019, 52(1): 91–99
133. Wang C, Wang C, Huang Z, Xu S. Materials and structures toward soft electronics toward soft electronics. Advanced Materials, 2018, 30(50): 1801368
134. Dickey M D. Stretchable and soft electronics using liquid metals. Advanced Materials, 2017, 29(27): 1606425–1606443
135. Kang S, Cho S, Shanker R, Lee H, Park J, Um D S, Lee Y, Ko H. Transparent and conductive nanomembranes with orthogonal silver nanowire arrays for skin-attachable loudspeakers and microphones. Science Advances, 2018, 4(8): eaas8772
136. Liu J, Wang L. Liquid Metal 3D Printing: Principles and Application. Shanghai: Shanghai Science & Technology Press, 2018 (in Chinese)
137. Zheng Y, He Z, Gao Y, Liu J. Direct desktop printed-circuits-on-paper flexible electronics. Scientific Reports, 2013, 3(1): 1786
138. Zhang Q, Gao Y, Liu J. Atomized spraying of liquid metal droplets on desired substrate surfaces as a generalized way for ubiquitous printed electronics. Applied Physics. A, Materials Science & Processing, 2014, 116(3): 1091–1097
139. Zheng Y, He Z Z, Yang J, Liu J. Personal electronics printing via tapping mode composite liquid metal ink delivery and adhesion mechanism. Scientific Reports, 2014, 4: 4588
140. Wang X, Liu J. Recent advancements in liquid metal fexible printed electronics: properties, technologies, and applications. Micromachines, 2016, 7(12): 206
141. Wang Q, Yu Y, Yang J, Liu J. Fast fabrication of flexible functional crcuits based on liquid metal dual-trans printing. Advanced Materials, 2015, 27(44): 7109–7116
142. Boczkal G. Electrons charge concentration and melting point of bcc metals. Materials Letters, 2014, 134: 162–164
143. Gunawardana K G, Wilson S R, Mendelev M I, Song X. Theoretical calculation of the melting curve of Cu-Zr binary alloys. Physical Review, 2014, 90 (5–1): 052403
144. Boczkal G. Melting point of metals In relation to electron charge density. Archives of Metallurgy and Materials, 2015, 60 (3): 2457–2460